

ASCA X-ray source catalogue in the Galactic Center region

Masaaki Sakano^{1,2}

Department of Physics and Astronomy, University of Leicester, University Road, Leicester LE1 7RH, UK

sakano@cr.scphys.kyoto-u.ac.jp

and

Katsuji Koyama, Hiroshi Murakami²

Department of Physics, Kyoto University, Kyoto 606-8502 Japan,

koyama@cr.scphys.kyoto-u.ac.jp

,

hiro@cr.scphys.kyoto-u.ac.jp

and

Yoshitomo Maeda^{2,3,4}

Institute of Space and Astronautical Science (ISAS), Kanagawa 229-8510 Japan,

maeda@astro.psu.edu

and

Shigeo Yamauchi

Faculty of Humanities and Social Sciences, Iwate University, 3-18-34 Ueda, Morioka, Iwate 020-8550 Japan,

yamauchi@iwate-u.ac.jp

¹Space Utilization Research Program (SURP), National Space Develop Agency of Japan (NASDA), 2-1-1 Sengen, Tsukuba, Ibaraki 305-8505 Japan

²Research Fellow of the Japan Society for the Promotion of Science.

³Subaru Telescope,National Astronomical Observatory of Japan, 650 North Aohoku Place, Hilo, HI 96720

⁴Department of Astronomy and Astrophysics, The Pennsylvania State University, 525 Davey Lab., University park, PA 16802-6305

ABSTRACT

The *ASCA* satellite made 107 pointing observations on a 5×5 deg 2 region around the center of our Milky Way Galaxy (the Galactic Center) from 1993 to 1999. In the X-ray images of the 0.7–3 keV or 3–10 keV bands, we found 52 point sources and a dozen diffuse sources. All the point sources are uniformly fitted with an absorbed power-law model. For selected bright sources, Sgr A*, AX J1745.6–2901, A 1742–294, SLX 1744–300, GRO J1744–28, SLX 1737–282, GRS 1734–292, AX J1749.2–2725, KS 1741–293, GRS 1741.9–2853, and an unusual flare source XTE J1739–302, we present further detailed spectral and timing analyses, and discuss their nature. The dozen extended X-ray sources comprise radio supernova remnants, giant molecular clouds, and some new discoveries. Most show emission lines from either highly ionized atoms or low-ionized irons. The X-ray spectra were fitted with either a thin thermal or power-law model. This paper summarizes the results and provides the *ASCA* X-ray source catalogue in the Galactic Center region.

Subject headings: catalogs — surveys — Galaxy: center — X-rays: general — X-rays: stars — stars: general

1. INTRODUCTION

Stars, hot gas, and cold gas are densely distributed near the center of galaxies, which may lead to various activities, e.g., mass accretion on a massive black hole, starbursts, and supernova explosions. These phenomena are also suggested in the center of our Milky Way galaxy, the Galactic Center region. Its proximity to us makes the Galactic Center region an excellent laboratory for the most detailed study on such activity, hence it has been one of the major research objects (see reviews by Morris & Serabyn 1996; Mezger, Duschl, & Zylka 1996).

Hard X-rays are key wavelengths for the study of the Galactic Center activity because a putative massive black hole, starbursts, and their relics are all potential X-ray emitters, and those X-rays are almost free from interstellar absorption. Initially, hard X-ray studies have been made with non-imaging instruments (no mirror) (e.g., Kellogg et al. 1971; Proctor et al. 1978; Skinner et al. 1987; Kawai et al. 1988; Yamauchi et al. 1990; Sunyaev et al. 1991b; Sunyaev, Markevitch, & Pavlinsky 1993; Pavlinsky, Grebenev, & Sunyaev 1994; Churazov et al. 1994).

The most distinct components in the Galactic Center region were variable point sources (e.g., Pavlinsky et al. 1994), which are binaries with black holes or neutron stars, and the Galactic nucleus. Other than the point sources, supernova remnants (SNRs) and largely extended high-temperature plasma were also found (e.g., Koyama et al. 1989). Most of the previous instruments, however, suffered from severe source-confusion problem in the crowded Galactic Center region.

ASCA is the first satellite equipped with X-ray mirrors and detectors that have a high sensitivity and reasonable spectral and spatial resolutions in the wide energy band up to 10 keV, hence has been used for more detailed imaging spectroscopy in the Galactic Center region (e.g., Koyama et al. 1996; Maeda & Koyama 1996; Maeda 1998; Tanaka et al. 2000; Sakano 2000). The next hard X-ray mirror satellite, *Beppo-SAX*, also revealed new high-energy aspects near the Galactic Center region (Sidoli et al. 1999).

These works, however, have been limited to individual X-ray sources. In order to obtain comprehensive and unbiased knowledge on the central 5×5 degree² region, we have performed a complete survey since 1998 with *ASCA*. This paper summarizes the results with the following order. Details for the observations and the data screening are given in §2. In §3, X-ray images of the Galactic Center region in the hard and soft energy bands are constructed. Section 4 provides the detected sources, their spectral parameters, and identifications. Further details for selected bright sources are presented in §5. Throughout this paper, we assume the distance to the Galactic Center to be 8.5 kpc.

2. OBSERVATIONS

ASCA has four X-ray telescopes (XRT) with focal plane detectors of two Solid State Imaging Spectrometers (SIS0 and 1) and two Gas Imaging Spectrometers (GIS2 and 3). Instrument details are found in Serlemitsos et al. (1995), Burke et al. (1991, 1994), Yamashita et al. (1997), Ohashi et al. (1996), Makishima et al. (1996), while a general description of *ASCA* can be found in Tanaka, Inoue, & Holt (1994).

Since the field of view of SIS is smaller than that of GIS, and the performance of the SISs has been significantly degraded since 1995 due to the radiation of charged particles (Dotani et al. 1997), this paper refers to the GIS data unless otherwise stated. The GISs were generally operated in the PH mode with the standard bit-assignment (10-8-8-5-0-0; see Ohashi et al. 1996), unless otherwise noted (Table 1).

The GIS fields at selected targets including 4 TOO (Target Of Opportunity) transient sources were observed with the pointing mode. In order to fill blank fields, we performed

follow-up survey observations from 1998 to 1999. In total, the Galactic Center $5^\circ \times 5^\circ$ region was observed 107 times from 1993 to 1999. Table 1 and Figure 1 summarize the observation log with the sequence numbers (Obs-ID, here and after). The total exposure time in the Galactic Center $5^\circ \times 5^\circ$ area is about 1600 ksec, however, the exposure for each GIS field scatters largely from 5 to 200 ksec, depending on the observation modes or objectives (targets). For the follow-up survey fields, shorter exposures (e.g., 10 ksec) were generally allocated, while longer exposures (e.g., 200 ksec) were achieved for multiple-pointings on selected target fields.

Data screening was performed, using the standard method described in Day et al. (1995). The data with telemetry saturation of larger than 2σ level are discarded, except for Obs-ID 27 field (see Table 1), where the telemetry saturation were corrected according to Nishiuchi et al. (1999). The rise-time discrimination was applied to reject non-X-ray background (NXB), except for Obs-ID=27 (see Table 1). For timing analyses, barycentric arrival time correction was made for all the X-ray photons.

3. X-RAY IMAGES

Figures 2a and 2b show the X-ray images in the Galactic Center $5^\circ \times 5^\circ$ region with the energy bands of 3.0–10.0 and 0.7–3.0 keV, respectively. A blank region around $(l_{\text{II}}, b_{\text{II}}) = (-1.5, -1.5)$ is due to unexpected accidents in the *ASCA* operation. A region around the brightest source GX3+1 is heavily contaminated by the stray light (see next paragraph), hence is deleted as is seen by a blank semi-circle around $(l_{\text{II}}, b_{\text{II}}) = (2.3, 0.8)$. For the same reason, some pointing data for extremely bright transient sources, such as the flare data of GRO J1744–28, are discarded.

In the hard energy band of 3–10 keV (Fig. 2a), the brightest are X-ray point sources. Radial structures seen around $(l_{\text{II}}, b_{\text{II}}) = (-0.2, -0.8)$ and $(0.6, 1.0)$ are artifacts made by the stray lights from the bright sources. Since the stray lights are time variable, some artificial discontinuity cannot be removed in the re-constructed image, or mosaic-image (e.g., Serlemitsos et al. 1995).

Ignoring the artificial structures around bright point sources, we still see further diffuse structures, in particular near the Galactic plane. These are local enhancements of the hot plasma and X-ray reflection nebulae (Koyama et al. 1996; Maeda 1998; Maeda et al. 1999; Murakami et al. 1999, 2000a, 2000b, 2001; Sakano et al. 1999c, 2000a; Tanaka et al. 2000).

The X-ray image in the soft energy band (0.7–3 keV; Fig. 2b) is largely different from that of the hard energy band. The bright hard-band point sources, located near the Galactic

plane, become fainter due to the heavy absorption (e.g., Sakano et al. 1999b; Sakano 2000). Diffuse clumpy structures are clearer than that in the hard band. The stray light structures become dim, due simply to the reduced flux of the original point sources.

4. X-RAY SOURCE LIST IN THE GALACTIC CENTER REGION

Since the diffuse background and stray light structures are complex, source detection cannot be a simple job. We therefore developed the source detection procedures following the method by Ueda et al. (1998, 1999).

We first pick up source candidates from each pointing image. This procedure can resolve neighboring sources separated as small as 1 arcmin. We then determine the accurate source positions by a 2-dimensional image-fitting of the raw GIS2+3 image, using the relevant point spread function (PSF) and the background taken from the off-plane blank sky. The normalization of the background is allowed to be free. We apply the fitting to narrow regions with the size of $10' \times 10'$ centered at the source to minimize the spatial fluctuation of the background in the fitting region. These source finding procedures are applied separately to the soft-band (0.7–3.0 keV) and the hard-band (3.0–10.0 keV) images of each observation.

Although the statistical errors of the positions are less than $10''$, the systematic errors due to the background fluctuation and the calibration uncertainty is far larger, particularly near the edge of the GIS field. Thus, the nominal positional error radius is $50''$ in 90% confidence.

For each of the candidate sources, we accumulate the spectrum from a circle with a radius of $3'$. The background spectrum is made from the annular region with radii of $3'-5'$ centered at the source position. In these accumulations, we reject the pixels located within $2'$ from nearby source candidates or diffuse enhancements. We define the significance to be the ratio of the source counts to the 1σ fluctuation of the relevant background, and set the source detection criteria to be at the 5σ level.

Above procedures occasionally picked up “false” sources from bright diffuse structures, either real diffuse or stray light, as candidates of a point source or superposition of point sources. We therefore inspected all the source images and removed the “false” candidates from the source catalogue.

Each source spectrum was fitted with an absorbed power-law function. When the spectral parameters were not constrained, we used the best-fit values obtained with the best-quality spectrum (for multiple pointing) or fixed them to the lower-limit or upper-limit

values, and estimated the 0.7–10 keV flux. All the results are summarized in Table 2.

The source identification and the counterpart search were made, using the past references and the SIMBAD database. Thirty-one sources are found to have a counterpart. The results are listed in Table 2.

By the inspection of the X-ray image and discarding the stray light structures, we found a dozen diffuse X-ray sources. Most of them are X-rays from radio SNRs, but some are new discoveries. The spectra are fitted with an absorbed thin thermal plasma model or a power-law function (and emission lines). The best-fit parameters and other relevant information are summarized in Table 3.

5. NATURE OF SELECTED BRIGHT SOURCES

5.1. Sgr A* & AX J1745.6–2901

ASCA has observed the Sgr A region four times (see Table 2): twice in 1993 (Obs-ID=2, 7), once in 1994 (Obs-ID=12) and in 1997 (Obs-ID=39). The observation span is thus 3.5 yrs, which is the longest monitoring of Sgr A ever achieved by hard X-ray imaging instruments. We thus study long-term behaviors of X-ray sources in the Sgr A region. Since Koyama et al. (1996) reported that the spatial structure near to Sgr A is highly complicated, we analyze the data taken with the SIS detector, of which the spatial resolution is better than that of GIS. The SIS data are available in three of the four observations (Obs-IDs of 2, 12, and 39). Since the detailed results about the 1993 and 1994 data were already reported by Maeda et al. (1996) and Koyama et al. (1996), we mainly concentrate on the 1997 data unless otherwise stated.

Figure 3 shows an SIS image in 1997 for the 3–10 keV band. Two X-ray sources seen in the 1993 and 1994 data (Koyama et al. 1996; Maeda et al. 1996) also appeared in 1997; the north-east source (here and after, the Sgr A diffuse) is slightly extended (\sim a few arcmin), of which the spatial peak is consistent with Sgr A*, while the south-west source is a low mass X-ray binary AX J1745.6–2901, named by Kennea & Skinner (1996). The Sgr A diffuse showed no flux variation (see §5.1.2) while AX J1745.6–2901 was variable; the persistent fluxes of AX J1745.6–2901 in the 2–10 keV band were 1.2, 6.8, and 1.5×10^{-11} erg cm $^{-2}$ s $^{-1}$ in 1993, 1994 and 1997, respectively. We thus found that AX J1745.6–2901 was in the low-flux state in 1993 and 1997, and in the high state in 1994. Figure 4 summarizes the variabilities of both the sources.

5.1.1. AX J1745.6–2901

Maeda et al. (1996) discovered intensity dips with the interval of 8.356 ± 0.008 hr due to the eclipse from this source in the 1994 data. We newly analyze the 1997 data. We extracted X-ray photons from a circular region with a radius of $0'.8$, and made a light curve, just the same as Maeda et al. (1996). Then, we folded the light curves with 8.356 hr, and found a possible dip also in 1997 (Fig. 5). Note that non-detection of the dip in 1993 is probably due to its short exposure of 17 ksec, which is about one-quarter of that in 1997 (70 ksec).

To constrain the orbital period, we determined the center of the eclipsing phase to be MJD 49610.2326(2) and MJD 50523.275(1) in the 1994 and 1997 observations, respectively, by assuming a well-type light curve for the eclipse. The time interval between these two eclipse-centers is then 913.043(1) days. When no change of the orbital period is assumed, this time interval should be $P \times N$, where P is the orbital period and N is an integer. From the period of 8.356 ± 0.008 hr constrained by Maeda et al. (1996), we derived more accurate orbital period to be either 8.34782, 8.35100, 8.35419, 8.35737, 8.36056 or 8.36375 hrs with each error of 0.00001 hr.

5.1.2. The Sgr A Diffuse

We made the SIS spectra of the Sgr A diffuse for the three observations. All of the data in the 1993 observation (Obs-ID=2) were available, whereas those for the 1994 and 1997 observations were not. For the 1994 observation, only the data during the eclipse phase of AX J1745.6–2901 were used, because X-rays from AX J1745.6–2901 in non-eclipse phase, of which the flux was an order of magnitude larger than that of the Sgr A diffuse, highly contaminated the Sgr A diffuse spectrum. For the 1997 observation, we used only the 1-CCD-mode data, in which the energy resolution was much better than that in the 4-CCD-mode (Yamashita et al. 1997). The effective exposure time is then reduced to be 18, 2.5, 37 ksec for the 1993, 1994, and 1997 data, respectively.

For all the three observations, the spectra of the Sgr A diffuse and the background were taken from the paired regions given in Figure 3. By subtracting the background data, we removed spill-over X-rays from AX J1745.6–2901 and another transient source GRO J1744–28 only seen in 1997.

Figure 6 shows the background-subtracted spectrum in 1993, which has by far the best quality in these observations. We fitted the spectrum in 1993 with a model of bremsstrahlung and Gaussian lines. From the line energies, we can identify these lines as $K\alpha$ transitions of highly ionized ions of silicon, sulfur, argon, calcium, and iron atoms. We then fitted

the spectrum again, fixing the center energies of each line to the theoretical values, and determined the line fluxes. The best-fit parameters are listed in Table 4.

Thus, we quantitatively confirm the existence of optically thin thermal plasma just surrounding Sgr A*, which was initially reported by Koyama et al. (1996). The best-fit electron temperature is as high as ~ 8 keV, which is consistent with those reported by Koyama et al. (1996) and Sidoli & Mereghetti (1999). For the Galactic Center plasma extending over the 1-degree square region, Koyama et al. (1996) reported the prominent 6.4- and 6.97-keV lines, which are $K\alpha$ emission of cold and hydrogen-like iron, respectively. Therefore, we included these two lines in the fitting, but obtained no significant line fluxes (Table 4).

In order to study flux variations of the Sgr A diffuse, we fitted the spectra taken in 1994 and 1997 with the same model given in Table 4, allowing only the global normalization factor to be adjusted. The model well reproduced the spectral shapes of the two spectra. The best-fit fluxes of the three observations were constant within the statistical error, $\sim 2 \times 10^{-11}$ erg s $^{-1}$ cm $^{-2}$ (2–10 keV). Hence, the flux and the spectral shape of the Sgr A diffuse should be steady in the long time-span of the three observations (Fig. 4).

5.1.3. Sgr A*

The Sgr A diffuse, peaked at Sgr A*, is dominated by diffuse emission. With the three observations, the Sgr A diffuse showed no time-variability, which suggests that Sgr A* emits no significant point-like X-ray; the conservative upper-limit of the X-ray flux of Sgr A* is $F_{X,\text{Sgr A}^*} < 2 \times 10^{-11}$ erg cm $^{-2}$ s $^{-1}$ (2–10 keV). The X-ray luminosity of Sgr A* corrected for the interstellar absorption of 7×10^{22} H cm $^{-2}$ is then calculated to be $L_{X,\text{Sgr A}^*} < 3 \times 10^{35}$ erg s $^{-1}$ (2–10 keV). This upper limit is consistent with that measured with *SAX* (3×10^{35} erg s $^{-1}$; Sidoli & Mereghetti 1999) and the positive flux recently reported with *Chandra* (2×10^{33} erg s $^{-1}$; Baganoff et al. 2001).

Many hard X-ray observations near to Sgr A* with the non-imaging instruments had been performed before *ASCA* observations (for a summary of these observations, see Maeda et al. 1996). These observations suggested a long-term time-variability of Sgr A* with the 3–10 keV flux ranging $(1\text{--}16) \times 10^{-11}$ erg s $^{-1}$ cm $^{-2}$, which corresponds to the absorption-corrected luminosity of about $(1\text{--}20) \times 10^{35}$ erg s $^{-1}$ (Skinner et al. 1987; Kawai et al. 1988; Sunyaev et al. 1991a). Our *ASCA* monitoring over four years found that the low mass X-ray binary AX J1745.6–2901 is always present, which supports the argument by Maeda et al. (1996) that the X-ray fluxes previously reported with non-imaging instruments might have suffered from possible contamination of this source. If the flux-change were due to

AX J1745.6–2901, the periodic eclipse should be detected when the Sgr A region is in high state. However, ART-P reported no eclipse in the high state (Sunyaev et al. 1991a); and accordingly the variability would not be likely due to AX J1745.6–2901, but possibly due to Sgr A* (R. Sunyaev, private communication). In fact, the first *Chandra* observation reports a hint of variability for a small flare from Sgr A* (Baganoff et al. 2001) although the flux level is an order of 10^{33} erg s $^{-1}$. Presence of the moderately large variability should be tested by future *Chandra* and *XMM-Newton* observations.

5.2. A 1742–294, SLX 1744–300 & GRO J1744–28

We found 11 X-ray bursts from A 1742–294. The X-ray features are characteristic to the type-I bursts, hence we confirmed the previous results (e.g., Lewin et al. 1976)

We clearly resolved SLX 1744–300 from a nearby burster, SLX 1744–299 (Pavlinsky et al. 1994) separated by 3'. Although we found 11 bursts from SLX 1744–300, no burst was detected from SLX 1744–299. SLX 1744–300 is known to exhibit X-ray bursts with complicated profiles (Skinner et al. 1990, Pavlinsky et al. 1994). The detailed natures of the bursts, however, were not studied with *ASCA* due to the limited statistics.

GRO J1744–28 is a type-II burster and a 0.47 s pulsar with an orbital period of 11.83 days (e.g., Finger et al. 1996; Kouveliotou et al. 1996). Detailed natures with the *ASCA* observations on and before 1997 March are found in Nishiuchi et al. (1999). This source was observed again on 1998 September 7 (Obs-ID=55 & 56) with *ASCA*, but no significant flux was detected with the 3σ upper limit of 2×10^{-12} erg cm $^{-2}$ s $^{-1}$.

5.3. XTE J1739–302

A transient source XTE J1739–302 was discovered with *XTE* at ($17^{\text{h}}39^{\text{m}}00^{\text{s}}$, $-30^{\circ}16'.2$ (J2000)) on 1997 August 12 (Smith et al. 1997, 1998b). Although it was the brightest source in the Galactic Center region on August 12 ($\sim 3.0 \times 10^{-9}$ erg cm $^{-2}$ s $^{-1}$ from 2 to 25 keV), it was below the detection limit on 9 days before and 2 days after the flare. The *SAX*/WFC observation made on 1997 September 6 (Smith et al. 1998b) found no flux from this source.

We detected this source again with *ASCA* on 1999 March 11 (Obs-ID=76). Figure 7 shows the light curve in the 2–10 keV band. Two flares, which started at around MJD 51248.319, were detected.

The light curve was unusual; it showed no flux, then suddenly flared up and reached

the peak after 200–250 s, dropped to no flux level with the same time scale as the flare-rise (200–250 s). The second flare had the almost identical profile except the peak flux of about a half of that of the first flare. No significant difference in the light curves is found between the hard (4–10 keV) and the soft (1–4 keV) energy bands.

We accumulated the spectrum only during the flare. The spectrum is well fitted ($\chi^2/\text{dof} = 91.4/77$) with an absorbed power-law function of a photon index $\Gamma = 0.80_{-0.11}^{+0.10}$ and a hydrogen column density $N_{\text{H}} = 3.17_{-0.31}^{+0.33} \times 10^{22} \text{ H cm}^{-2}$. On the other hand, Smith et al. (1998b) reported that the *XTE* spectrum on 1997 August 12 was well described with a thermal bremsstrahlung model of $kT = 12.4 \pm 0.3$ keV. Hence, the *ASCA* result of the flat spectrum is very different from the *XTE* result; we note that the power-law index obtained with *ASCA* corresponds to a temperature over 100 keV when a bremsstrahlung model is applied. The column density is also different from the *XTE*/PCA result of $(5\text{--}6) \times 10^{22} \text{ H cm}^{-2}$ (Smith et al. 1998b). Thus, the spectral shape may have largely changed between the *XTE* and the *ASCA* observations.

We made the X-ray images in the pre-flare phase, and found no X-ray flux at the source position with the 3σ flux upper limit of $9 \times 10^{-13} \text{ erg cm}^{-2} \text{ s}^{-1}$ in the 2–10 keV band, assuming the same spectral shape during the flare phase. Since the peak flux of the first flare is about $2 \times 10^{-9} \text{ erg cm}^{-2} \text{ s}^{-1}$, this source exhibited drastic flux-increase by more than three orders within a few hundred seconds. The flat spectrum, highly variable flux, and absorption resemble those of transient pulsars. We accordingly searched for pulsation in time scales of 1–100 s with FFT analysis, and epoch folding for time scales of 100–1000 s, but found no significant pulsation, which is consistent with the *XTE* result by Smith et al. (1998b).

5.4. SLX 1737–282

The nature of SLX 1737–282 (Skinner et al. 1987), whether or not this is a persistent source, has been unknown. We observed SLX 1737–282 (AX J1747.0–2818) five occasions from 1996 to 1999, and always detected positive flux. The position is determined to be $(l_{\text{II}}, b_{\text{II}}) = (359^{\circ} 971, 1^{\circ} 231)$ with an error radius of $40''$, which is within the error radius of the *Einstein* measurement (Skinner et al. 1987). Therefore, we identified AX J1747.0–2818 as SLX 1737–282.

The 2–10 keV flux of SLX 1737–282 was measured to be $(3.5\text{--}5.0) \times 10^{-11} \text{ erg cm}^{-2} \text{ s}^{-1}$ through the five *ASCA* observations. Thus, SLX 1737–282 seems fairly stable in the long time span, but exhibited short time variability of $10^3\text{--}10^4$ seconds with amplitude of 100% in the *ASCA* observations.

The spectral shape had been also stable through 2.5-yr observations with a power-law function of a photon index $\Gamma = 2.1\text{--}2.4$ and a hydrogen column density $N_{\text{H}} = (1.8\text{--}2.2) \times 10^{22} \text{ H cm}^{-2}$. This column density implies that the distance of this source may be several kpc or farther. The absorption-corrected luminosity in the 2–10 keV band is $(4\text{--}7) \times 10^{35} \text{ erg s}^{-1}$ for the assumed distance of 8.5 kpc.

The power-law index, moderate variability, and the luminosity suggest that this source is a neutron star binary, although the other possibilities, such as an AGN, are not totally excluded.

5.5. GRS 1734–292

GRS 1734–292 was discovered with *Granat*/ART-P in 1990 by Sunyaev (1990b). Since then, it has been observed in the wide energy band, from the soft X-ray band below 2 keV (Barret & Grindlay 1996) to the hard X-ray band (Pavlinsky et al. 1994), even up to 400 keV (Churazov et al. 1992). Martí et al. (1998) found this source to be a radio jet-like source, NVSS J173728–290802, and further identified it to be a Seyfert 1 galaxy with $z = 0.0214$, combining the radio, optical, infrared, and X-ray results.

With *ASCA*, the X-ray emission from this source has been always clearly detected whenever we observed this source; accordingly, GRS 1734–292 is probably a persistent X-ray source. The X-ray spectrum was well represented with a power-law function of a photon index of 1.3–1.7 and a hydrogen column density $N_{\text{H}} = (1.3\text{--}2.0) \times 10^{22} \text{ H cm}^{-2}$.

The power-law index of 1.3–1.7 is within the nominal range of that of Seyfert 1s. The column density of $(1.3\text{--}2.0) \times 10^{22} \text{ H cm}^{-2}$ is significantly smaller than $N_{\text{H}} \sim 6 \times 10^{22} \text{ H cm}^{-2}$ determined with *Granat*/ART-P (Pavlinsky et al. 1994), but is consistent with the result of Martí et al. (1998), who estimated $N_{\text{H}} = (1.0 \pm 0.2) \times 10^{22} \text{ H cm}^{-2}$ based on the measurement of optical extinction and several absorption lines. Therefore, our results support the Seyfert 1 identification by Martí et al. (1998).

5.6. AX J1749.2–2725

This source was discovered with *ASCA* in 1995. Torii et al. (1998) found coherent pulsations of $P = 220.38 \pm 0.20 \text{ s}$ and $P = 220.44 \pm 0.80 \text{ s}$ periods in the Obs-ID=19, and Obs-ID=23 & 24 observations, respectively. The energy spectrum was described with a flat power-law function (photon index of $\Gamma = 0.7\text{--}1.3$) with heavy absorption ($N_{\text{H}} = (7\text{--}13) \times 10^{22} \text{ H cm}^{-2}$) through the *ASCA* observations until 1997.

We analyzed the data of Obs-ID=46 in 1998 March and confirmed the pulsations of $P = 219.9 \pm 1.0$ s period. Since the error of the pulse period was large, we found no significant \dot{P} from the previous observations. The spectral parameters except the flux were also consistent in each observation. The flux of 1×10^{-11} erg cm $^{-2}$ s $^{-1}$ was a few times smaller than that in 1995 March (Obs-ID=19) and September (Obs-ID=23&24), but a few times larger than that in 1996 September (Obs-ID=33&34) and 1997 September (Obs-ID=43).

5.7. KS 1741–293 & GRS 1741.9–2853

KS 1741–293 and GRS 1741.9–2853 are X-ray bursters (in't Zand et al. 1991; Cocchi et al. 1999a). *ASCA* found two sources at the position of $(l_{\text{II}}, b_{\text{II}}) = (359^{\circ}5600, -0^{\circ}0825)$ and $(359^{\circ}9507, 0^{\circ}1126)$ with the error radii of 40''. KS 1741–293 and GRS 1741.9–2853 lie within these error circles (e.g., in't Zand et al. 1991, 1998; Mandrou 1990; Sunyaev 1990a; Pavlinsky et al. 1994).

Although these two are not persistent sources and although we found no burst from both the sources, the positional coincidence, the apparent brightness in their high states, and the spectral parameters strongly favor that AX J1744.8–2921 and AX J1745.0–2855 (Table 2) are identical with KS 1741–293 and GRS 1741.9–2853, respectively. We found that both the sources have showed apparent variability by a factor of 50 or more. The fluxes in the quiescent state were less than a few 10^{-12} erg cm $^{-2}$ s $^{-1}$ in the 0.7–10 keV band (see Table 2).

The authors express their thanks to the *ASCA* team, and particularly, the *ASCA* Galactic plane/center survey team. We are grateful to Dr. K. Torii and an anonymous referee for their valuable comments and suggestions. They appreciate the help of Dr. Y. Ueda, Dr. Y. Ishisaki, Mr. J. Yokogawa, and Dr. L. Angelini in the analysis. We acknowledge Mr. A. Hands for correcting English. M. S. thanks Prof. K. Nishikawa, Dr. H. Awaki, and Dr. T. Tsuru. M. S., H. M., and Y. M. are financially supported by the Japan Society for the Promotion of Science for Young Scientists. A part of this work was based on the data in the SIMBAD database.

REFERENCES

Baganoff, F., et al. 2001, ApJ, in press (astro-ph/0102151)
Bamba, A., Yokogawa, J., Sakano, M., & Koyama, K. 2000, PASJ, 52, 259

Barret, D., & Grindlay, J. E. 1996, A&A, 311, 239

Bouchet, L., et al. 1991, ApJ, 383, L45

Burke, B. E., Mountain, R. W., Daniels, P. J., & Dolat, V. S. 1994, IEEE Trans. Nuc. Sci., 41, 375

Burke, B. E., Mountain, R. W., Harrison, D. C., Bautz, M. W., Doty, J. P., Ricker, G. R., & Daniels, P. J. 1991, IEEE Trans., ED-38, 1069

Churazov, E., Gilfanov, M., Cordier, B., & Schmitz-Fraysse, M. C. 1992, IAU Circ. 5623

Churazov, E., Gilfanov, M., & Sunyaev, R. 1996, ApJ, 464, L71

Churazov, E., et al. 1994, ApJS, 92, 381

Churazov, E., et al. 1995, ApJ, 443, 341

Cocchi, M., Bazzano, A., Natalucci, L., Ubertini, P., Heise, J., Muller, J. M., & in't Zand, J. J. M. 1999a, A&A, 346, L45

Cocchi, M., in't Zand, J. J. M., Bazzano, A., Heise, J., Muller, J. M., Natalucci, L., & Ubertini, P. 1999b, Nucl. Phys. B, 69/1, 232

Cremonesi, D. I., Mereghetti, S., Sidoli, L., & Israel, G. L. 1999, A&A, 345, 826

Cui, W., Heindl, W. A., Swank, J. H., Smith, D. M., Morgan, E. H., Remillard, R., & Marshall, F. E. 1997, ApJ, 487, L73

David, P., Goldwurm, A., Murakami, T., Paul, J., Laurent, P., & Goldoni, P. 1997, A&A, 322, 229

Day, C., Arnaud, K., Ebisawa, K., Gotthelf, E., Ingham, J., Mukai, K., & White, N. 1995, the ABC guide to *ASCA* data reduction, NASA/GSFC

Dotani, T., Fujimoto, R., Nagase, F., & Inoue, H. 1995, IAU Circ. 6241

Dotani, T., Yamashita, A., Ezuka, H., Takahashi, K., Crew, G., Mukai, K., & the SIS Team 1997, The *ASCA* news (Greenbelt: NASA GSFC), 5, 14

Elvis, M., Plummer, D., Schachter, J., & Fabbiano, G. 1992, ApJS, 80, 257

Falcke, H., Cotera, A., Duschl, W. J., Melia, F., & Rieke, M. J. 1999, “The central parsecs of the Galaxy”, ASP Conf. Ser. 186,

Finger, M. H., Koh, D. T., Nelson, R. W., Prince, T. A., Vaughan, B. A., & Wilson, R. B. 1996, Nature, 381, 291

Ghez, A. M., Klein, B. L., Morris, M., & Becklin, E. E. 1998, ApJ, 509, 678

Goldwurm, A., et al. 1994, Nature, 371, 589

Gray, A. D. 1994, MNRAS, 270, 835

Green, D. A., & Gull, S. F. 1984, *Nature*, 312, 527

Heindl, W. A., Prince, T. A., & Grunsfeld, J. M. 1994, *ApJ*, 430, 829

Heise, J. 1997, *IAU Circ.* 6606

Helfand, D. J., & Becker, R. H. 1987, *ApJ*, 314, 203

Hjellming, R. M., et al. 1998, *A&AS*, 193, 10308

in't Zand, J., Heise, J., Smith, M., Muller, J. M., Ubertini, P., & Bazzano, A. 1998, *IAU Circ.* 6840

in't Zand, J. J. M., et al. 1991, *Advances in Space Research*, 11, 187

Kawai, N., Fenimore, E. E., Middleditch, J., Cruddace, R. G., Fritz, G. G., Snyder, W. A., & Ulmer, M. P. 1988, *ApJ*, 330, 130

Kellogg, G. H., Murray, S., Tananbaum, H., & Giacconi, R. 1971, *ApJ*, 169, L99

Kennea, J. A., & Skinner, G. K. 1996, *PASJ*, 48, L117

Kotani, T., et al. 2000, *ApJ*, 543, L133

Kouveliotou, C., et al. 1996, *Nature*, 379, 799

Koyama, K., et al. 1989, *Nature*, 339, 603

Koyama, K., Maeda, Y., Sonobe, T., Takeshima, T., Tanaka, Y., & Yamauchi, S. 1996, *PASJ*, 48, 249

Kuznetsov, S., et al. 1997, *MNRAS*, 292, 651

Lewin, W. H. G., et al. 1976, *MNRAS*, 177, 83

Lewin, W. H. G., Rutledge, R. E., Kommers, J. M., van Paradijs, J., & Kouveliotou, C. 1996, *ApJ*, 462, L39

Maeda, Y. 1998, Ph.D. thesis, Kyoto University

Maeda, Y., & Koyama, K. 1996, in proc of “the 4th ASP international meeting — The Galactic Center”, ed. R. Gredel (San Francisco: Astronomical Society of the Pacific (ASP)), 102, 423

Maeda, Y., Koyama, K., Sakano, M., Takeshima, T., & Yamauchi, S. 1996, *PASJ*, 48, 417

Maeda, Y., et al. 1999, *Astron. Nach.*, 320, 177

Makishima, K., et al. 1983, *ApJ*, 267, 310

Makishima, K., et al. 1996, *PASJ*, 48, 171

Mandrou, P. 1990, *IAU Circ.* 5032

Martí, J., Mirabel, I. F., Chaty, S., & Rodríguez, L. F. 1998, *A&A*, 330, 72

Mereghetti, S., Sidoli, L., & Israel, G. L. 1998, *A&A*, 331, L77

Mezger, P. G., Duschl, W. J., & Zylka, R. 1996, *A&A Rev.*, 7, 289

Mirabel, I. F., Rodríguez, L. F., Cordier, B., Paul, J., & Lebrun, F. 1992, *Nature*, 358, 215

Morris, M., & Serabyn, E. 1996, *ARA&A*, 34, 645

Murakami, H., Koyama, K., Maeda, Y., & Sakano, M. 1999, *Astron. Nach.*, 320, 325

Murakami, H., Koyama, K., Maeda, Y., Sakano, M., Nishiuchi, M., & Tsujimoto, M. 2000a, *Advances in Space Research*, 25(3/4), 575

Murakami, H., Koyama, K., Sakano, M., Tsujimoto, M., & Maeda, Y. 2000b, *ApJ*, 534, 283

Murakami, H., Koyama, K., Tsujimoto, M., Maeda, Y., & Sakano, M. 2001, *ApJ*, 550, 297

Nishiuchi, M., et al. 1999, *ApJ*, 517, 436

Ohashi, T., et al. 1996, *PASJ*, 48, 157

Pavlinsky, M. N., Grebenev, S. A., & Sunyaev, R. A. 1994, *ApJ*, 425, 110

Predehl, P., & Kulkarni, S. R. 1995, *A&A*, 294, L29

Proctor, R. J., Skinner, G. K., & Wilmore, A. P. 1978, *MNRAS*, 185, 745

The ROSAT Consortium 2000, “The ROSAT Source Catalog of Pointed Observations with the Position Sensitive Proportional Counter (2RXP)” in *ROSAT News No. 72*

Rupen, M. P., Hjellming, R. M., & Mioduszewski, A. J. 1998, *IAU Circ.* 6938

Sakano, M. 2000, Ph.D. thesis, Kyoto University

Sakano, M., Imanishi, K., Tsujimoto, M., Koyama, K., & Maeda, Y. 1999a, *ApJ*, 520, 316

Sakano, M., Koyama, K., Nishiuchi, M., Yokogawa, J., & Maeda, Y. 1999b, *Advances in Space Research*, 23(5/6), 969

Sakano, M., Koyama, K., Nishiuchi, M., Yokogawa, J., & Maeda, Y. 1999c, *Astron. Nach.*, 320, 330

Sakano, M., Koyama, K., Maeda, Y., & ASCA Galactic Plane Survey Team 2000a, *Advances in Space Research*, 25(3/4), 575

Sakano, M., Torii, K., Koyama, K., Maeda, Y., & Yamauchi, S. 2000b, *PASJ*, 52, 1141

Sakano, M., Yokogawa, J., Murakami, H., Koyama, K., Maeda, Y., & The ASCA Galactic Plane/Center Survey team 1999d, in proc of “the Japanese-German workshop on high energy astrophysics”, ed. W. Becker, & M. Itoh (MPE Report 270), 113

Scott, D. M., Finger, M. H., Wilson, R. B., Koh, D. T., Prince, T. A., Vaughan, B. A., & Chakrabarty, D. 1997, *ApJ*, 488, 831

Senda, A., Murakami, H., & Koyama, K. 2001, ApJ, submitted

Serlemitos, P. J., et al. 1995, PASJ, 47, 105

Sidoli, L., & Mereghetti, S. 1999, A&A, 349, L49

Sidoli, L., Mereghetti, S., Israel, G. L., Chiappetti, L., Treves, A., & Orlandini, M. 1999, ApJ, 525, 215

Skinner, G. K., Foster, A. J., Willmore, A. P., & Eyles, C. J. 1990, MNRAS, 243, 72

Skinner, G. K., Willmore, A. P., Eyles, C. J., Bertram, D., & Church, M. J. 1987, Nature, 330, 544

Smith, D. A., Levine, A., & Wood, A. 1998a, IAU Circ. 6932

Smith, D. M., Main, D., Marshall, F., Swank, J., Heindl, W., & Leventhal, M. 1997, IAU Circ. 6748

Smith, D. M., et al. 1998b, ApJ, 501, L181

Sunyaev, R. 1990a, IAU Circ. 5104

Sunyaev, R. 1990b, IAU Circ. 5123

Sunyaev, R., et al. 1991b, Advances in Space Research, 11, 177

Sunyaev, R. A., Markevitch, M., & Pavlinsky, M. 1993, ApJ, 407, 606

Sunyaev, R., et al. 1991a, Sov. Astron. Lett., 17, 42

Tanaka, Y., Inoue, H., & Holt, S. S. 1994, PASJ, 46, L37

Tanaka, Y., Koyama, K., Maeda, Y., & Sonobe, T. 2000, PASJ, 52, L25

Torii, K., et al. 1998, ApJ, 508, 854

Ueda, Y., et al. 1999, ApJ, 518, 656

Ueda, Y., et al. 1998, Astron. Nach., 319, 47

Voges, W., et al. 1999, A&A, 349, 389

Watson, M. G., Willingale, R., Hertz, P., & Grindlay, J. E. 1981, ApJ, 250, 142

Yamashita, A., et al. 1997, IEEE Trans. Nucl. Sci., 44, 847

Yamauchi, S., Kawada, M., Koyama, K., Kunieda, H., & Tawara, Y. 1990, ApJ, 365, 532

Yokogawa, J., Sakano, M., Koyama, K., & Yamauchi, S. 2000, Advances in Space Research, 25(3/4), 571

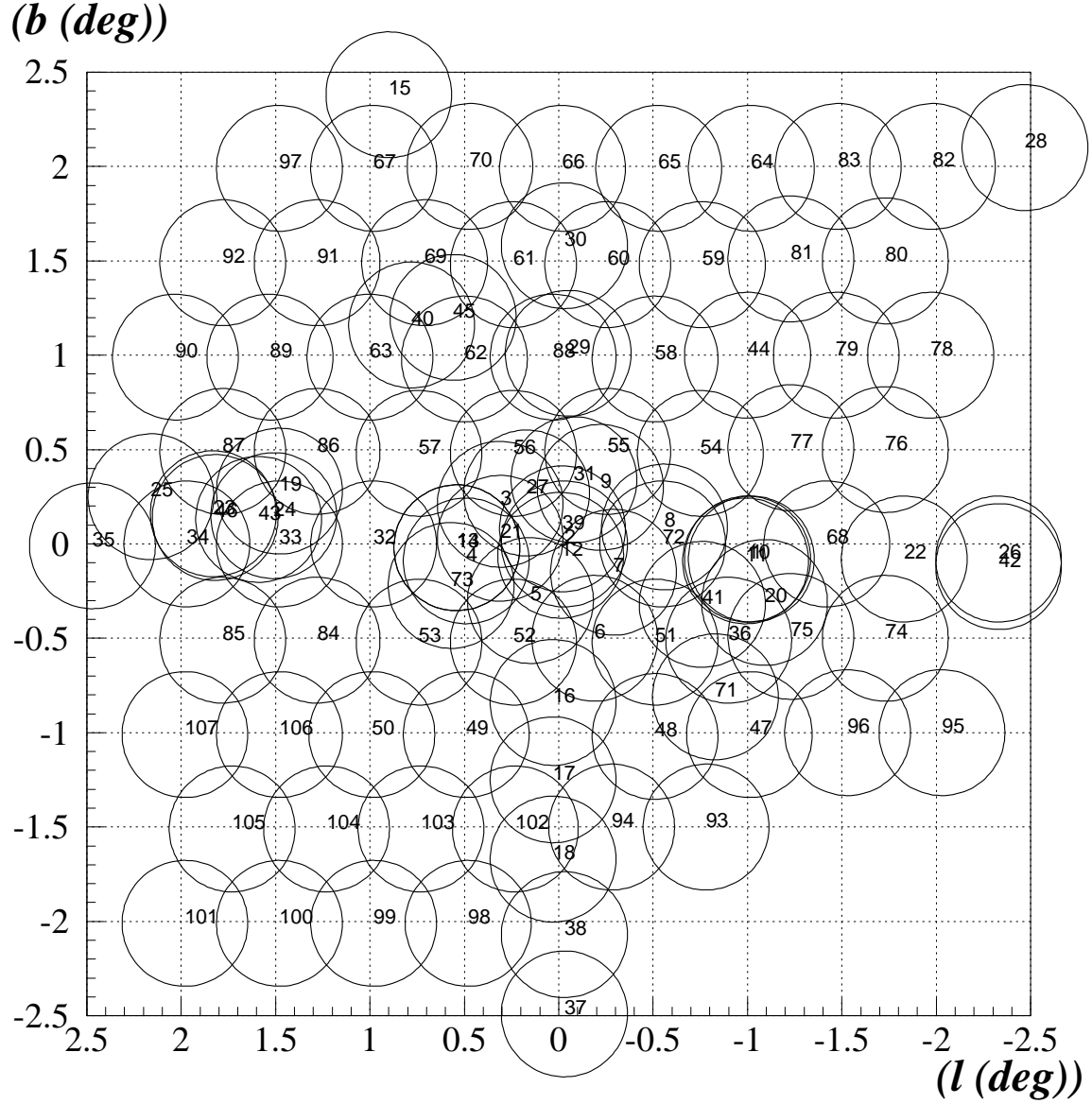


Fig. 1.— The GIS fields of view of all the *ASCA* pointings in the Galactic Center $5^\circ \times 5^\circ$ region with the galactic coordinates. The radius of each circle is $20'$. See Table 1 for the field IDs (Obs-IDs).

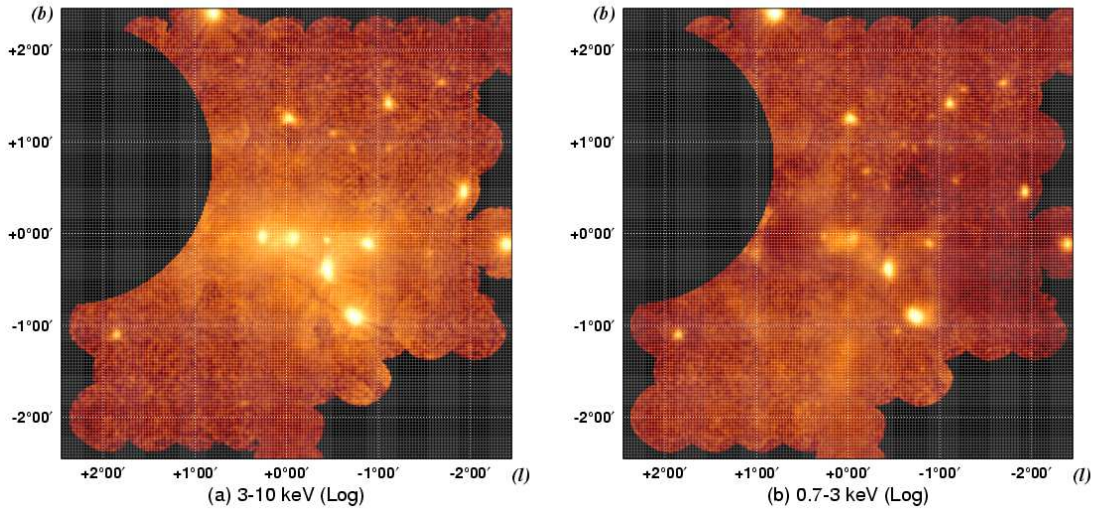


Fig. 2.— *ASCA* X-ray images in the Galactic Center $5^\circ \times 5^\circ$ region for the energy bands of (a) 3.0–10.0 and (b) 0.7–3.0 keV with the galactic coordinates. The color levels are logarithmically spaced. The data of GIS2 and GIS3 are summed, smoothed with a Gaussian filter of $\sigma = 3$ pixels (~ 0.75 arcmin), and corrected for exposure, vignetting, and the detection efficiency with GIS grid, after non-X-ray background is subtracted, according to the method described in Sakano (2000). A region around $(l_{\text{II}}, b_{\text{II}}) = (2^\circ.3, 0^\circ.8)$ is heavily contaminated by the stray light from GX 3+1, hence is deleted as is seen by a blank semi-circle.

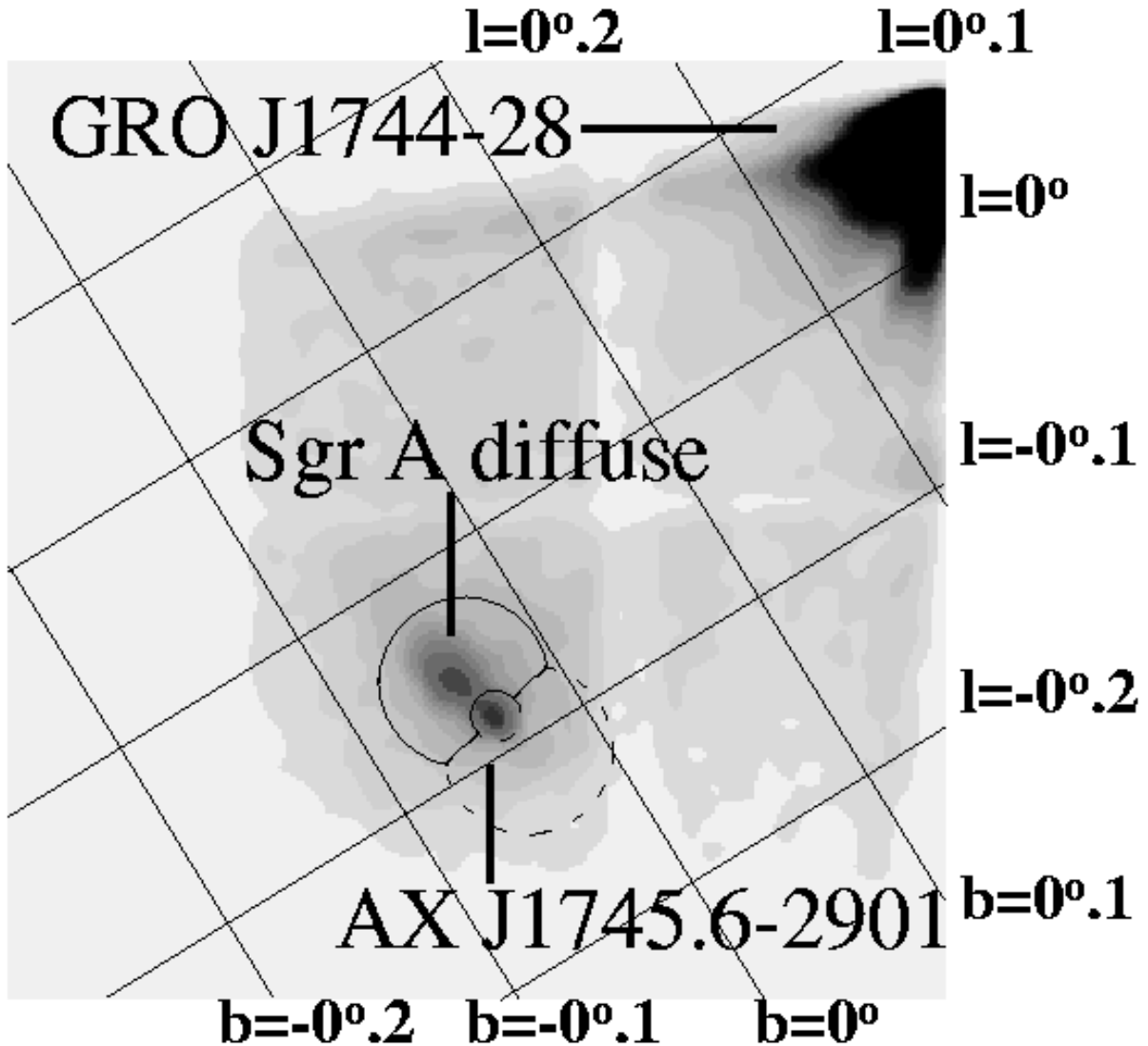


Fig. 3.— X-ray image of the Sgr A region for the 3–10 keV band in 1997 (Obs-ID=39) taken with the SIS 4-CCD mode. X-ray photons for the spectra of the Sgr A diffuse and the background are accumulated from the region encircled by solid and dashed lines, respectively. The central small circle with a radius of $0'8$ is not used for the source- or the background-spectrum for the Sgr A diffuse emission, but for the light-curve of AX J1745.6–2901.

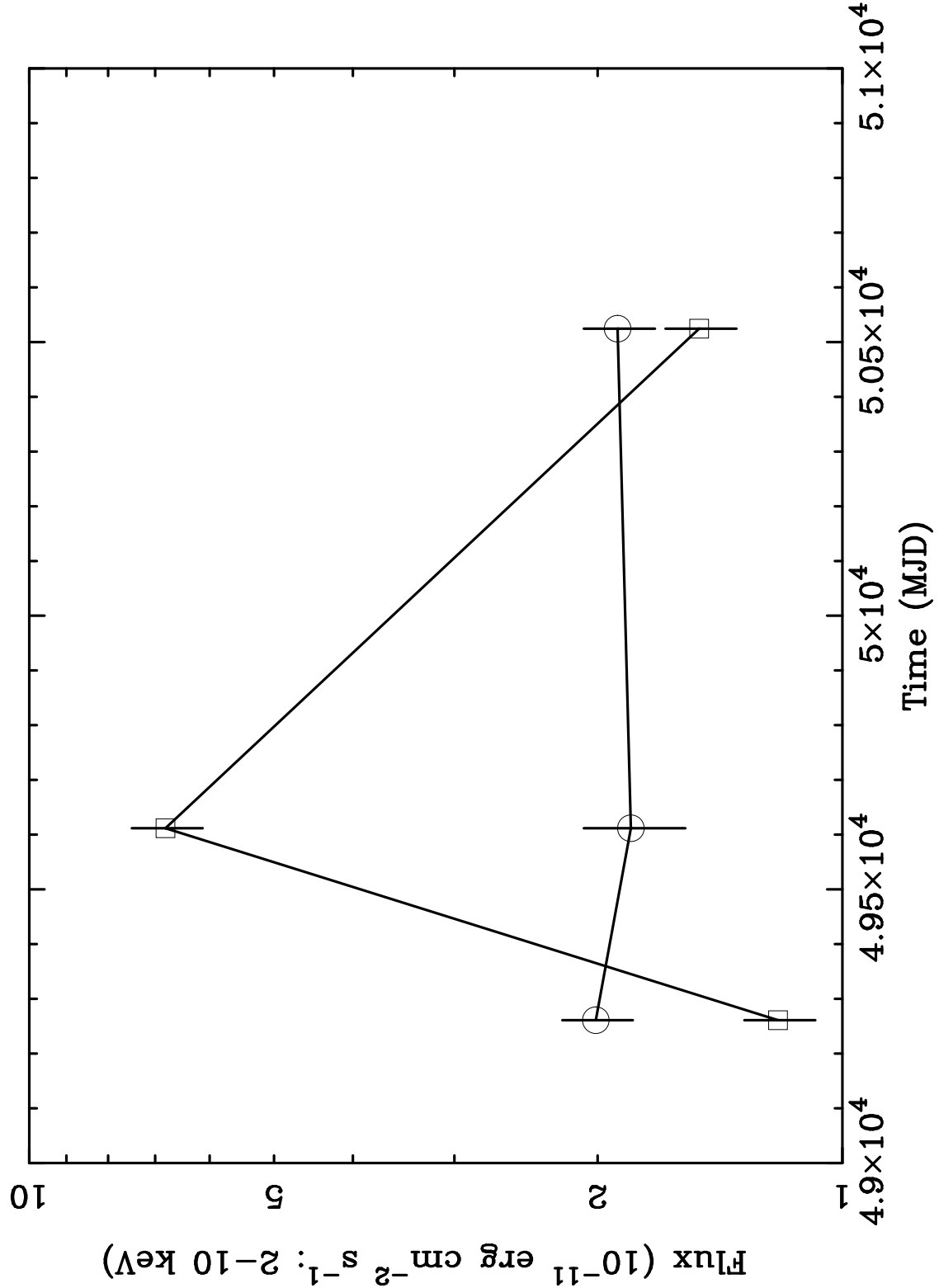


Fig. 4.— Flux histories of the Sgr A region (open circle) and AX J1745.6–2901 (open rectangle), observed with *ASCA*. The flux of the Sgr A region includes that of the Sgr A diffuse plasma and possible contribution from Sgr A*.

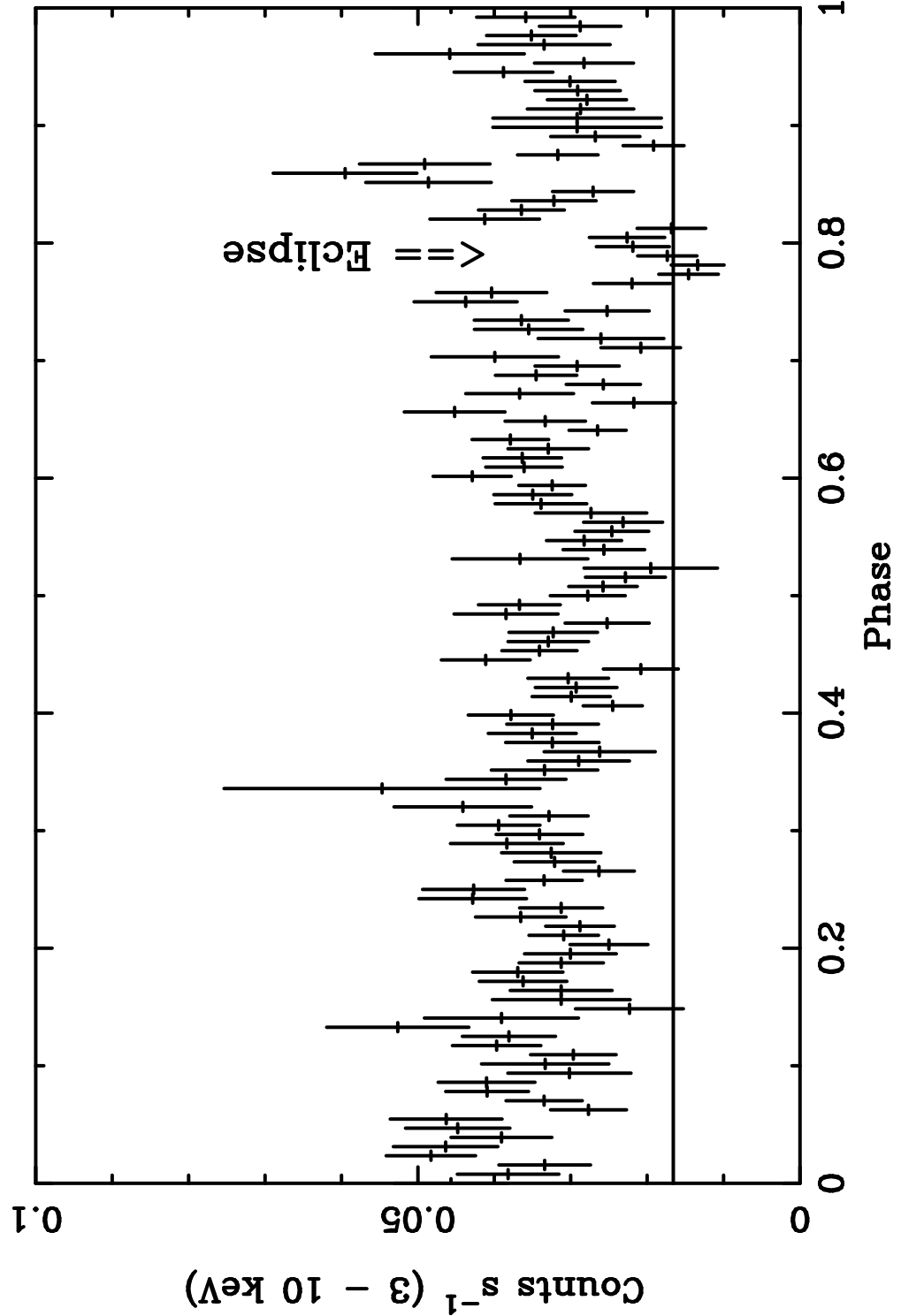


Fig. 5.— Folded light curve (3–10 keV) of AX J1745.6–2901 with the period of 8.356 hr in 1997 (Obs-ID=39) taken with SIS. The phase 0 epoch is set to MJD 50523.0. The solid line gives the background level. A possible dip corresponding to the eclipse can be seen.

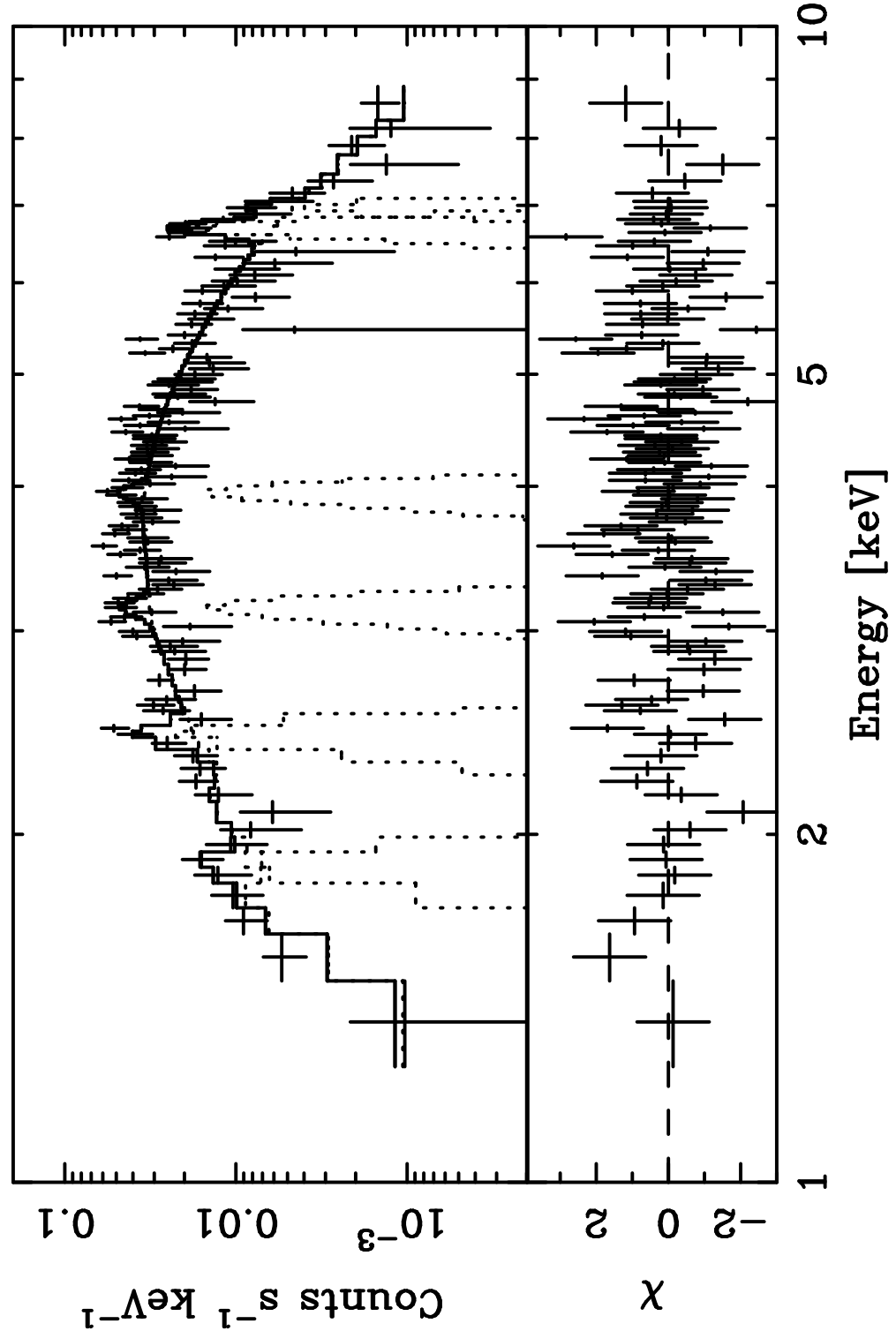


Fig. 6.— The SIS spectrum of the Sgr A diffuse in 1993 (Obs-ID=2). The spectrum is fitted with a model of bremsstrahlung and Gaussian lines.

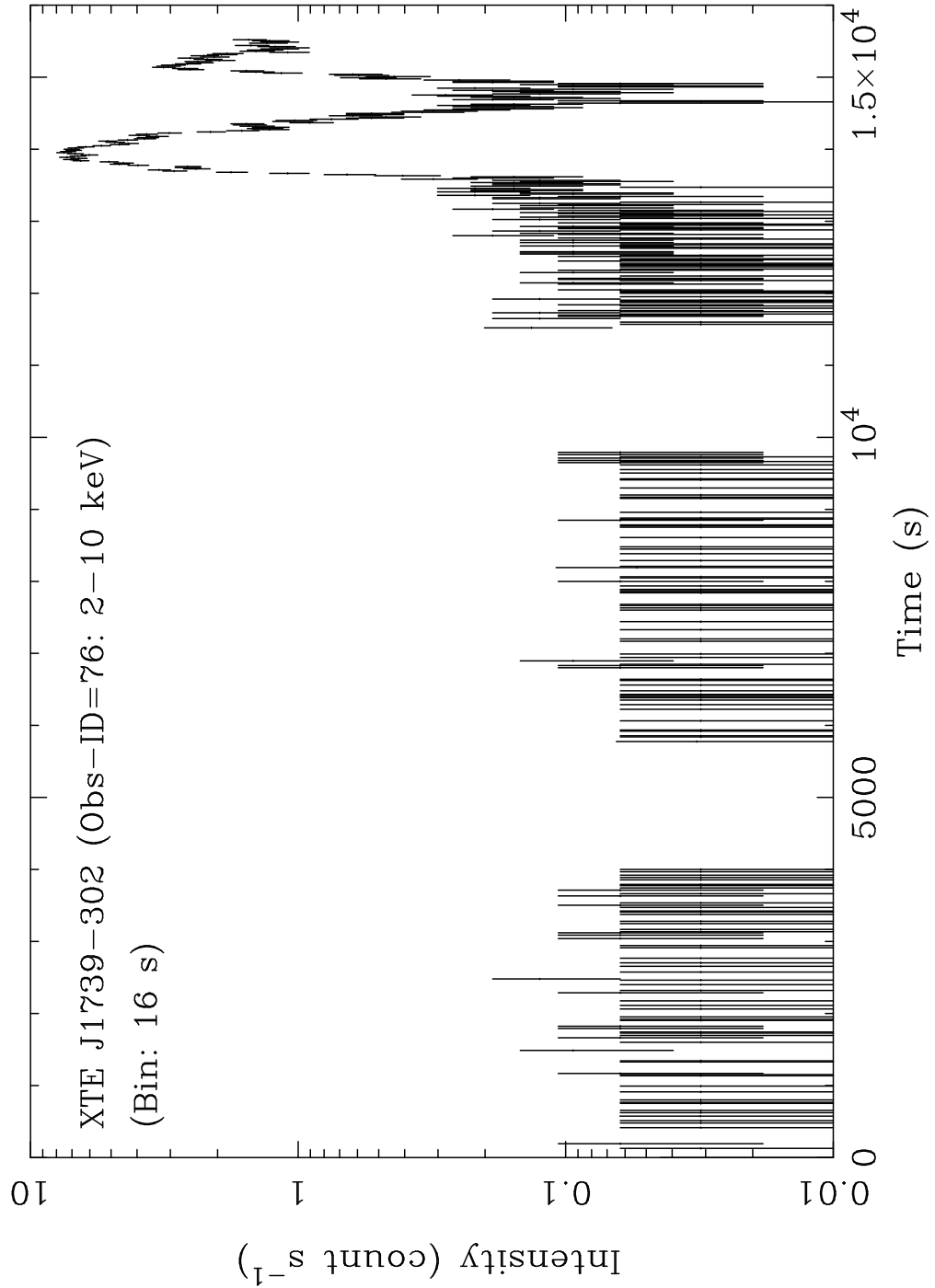


Fig. 7.— Light curve of XTE J1739–302 in the 2–10 keV band with 16 s bin. The vertical axis is the mean count rate of GIS 2 and GIS 3. The background is included, where the background level is $\sim 0.009 \text{ c s}^{-1}$. The start time is MJD 51248.163188.

Table 1. Observation log

Obs-ID	Date		Coordinates		Exp. ^a	Target name
	Start (UT) ^b	End (UT) ^b	l_{II} (deg.)	b_{II} (deg.)		
1	1993/09/26-00:12	1993/09/27-05:08	−1.02	−0.08	30.5	1E1740.7−294
2	1993/09/30-17:35	1993/10/01-07:27	−0.03	0.00	17.3	GC(0,0)
3	1993/10/01-07:06	1993/10/01-21:06	0.31	0.21	17.7	GC(0,−0.37)
4	1993/10/01-21:18	1993/10/02-10:14	0.49	−0.09	17.2	GC(0.37,−0.37)
5	1993/10/02-10:06	1993/10/03-00:58	0.15	−0.30	19.9	GC(0.37,0)
6	1993/10/03-00:30	1993/10/03-13:10	−0.19	−0.50	14.7	GC(0.37,0.37)
7	1993/10/03-13:34	1993/10/04-02:58	−0.29	−0.15	20.3	GC(0,0.37)
8	1993/10/04-02:54	1993/10/04-16:34	−0.56	0.09	19.8	GC(−0.37,0.37)
9	1993/10/04-16:29	1993/10/05-03:21	−0.22	0.30	17.9	GC(−0.37,0)
10	1994/09/08-19:40	1994/09/09-04:36	−1.00	−0.08	13.5	1E1740.7−2942 N1
11	1994/09/12-18:58	1994/09/13-01:06	−0.99	−0.09	11.8	1E1740.7−2942 N2
12	1994/09/15-22:46	1994/09/17-14:42	−0.01	−0.06	81.9	SGR A
13	1994/09/22-03:08	1994/09/23-12:48	0.54	−0.02	58.1	SGR B N1
14	1994/09/24-02:51	1994/09/24-14:11	0.54	−0.02	19.7	SGR B N2
15	1995/03/15-08:22	1995/03/15-22:06	0.90	2.38	18.6	SLX 1735−269
16	1995/03/21-03:44	1995/03/22-00:04	0.03	−0.84	25.1	GC(0min,−50min)
17	1995/03/22-00:00	1995/03/22-22:48	0.03	−1.25	27.0	GC(0min,−75min)
18	1995/03/22-22:44	1995/03/23-20:36	0.03	−1.67	25.3	GC(0min,−100min)
19	1995/03/26-03:31	1995/03/27-12:55	1.48	0.28	35.6	THE 200-PC RING N1
20	1995/03/27-12:50	1995/03/28-17:54	−1.09	−0.31	32.7	THE 200-PC RING N2
21	1995/09/19-08:54	1995/09/21-21:38	0.31	0.03	63.0	THE 6.4KEV ISLAND
22	1995/09/25-01:52	1995/09/25-08:36	−1.83	−0.08	8.6	GALACTIC RIDGE N1
23 ^c	1995/09/25-08:04	1995/09/25-14:08	1.83	0.16	5.0	GRO J1750−27 N1
24 ^c	1995/09/25-14:00	1995/09/25-17:20	1.51	0.15	2.5	GRO J1750−27 N2
25 ^c	1995/09/25-17:28	1995/09/26-00:44	2.16	0.25	8.9	GRO J1750−27 N3
26	1995/09/26-00:44	1995/09/26-09:00	−2.33	−0.08	12.7	GALACTIC RIDGE N2
27 ^c	1996/02/26-10:55	1996/02/27-02:47	0.17	0.27	14.0	GRO J1744−28
28	1996/03/08-17:19	1996/03/09-10:03	−2.47	2.10	19.2	HP 1
29	1996/09/10-03:56	1996/09/10-19:52	−0.05	1.01	13.4	LB=0 75
30	1996/09/10-19:20	1996/09/11-07:52	−0.03	1.58	18.8	LB=0 100
31 ^d	1996/09/11-07:47	1996/09/11-21:27	−0.08	0.34	16.8	LB=0 50
32	1996/09/19-15:21	1996/09/19-22:33	0.98	0.00	8.2	GAL RIDGE2 N1
33	1996/09/19-21:29	1996/09/20-04:33	1.48	0.00	10.7	GAL RIDGE2 N2
34	1996/09/20-04:29	1996/09/20-09:21	1.97	0.00	7.7	GAL RIDGE2 N3
35	1996/09/20-08:45	1996/09/20-13:25	2.47	−0.01	8.8	GAL RIDGE2 N4
36	1996/09/23-14:36	1996/09/24-02:32	−0.90	−0.51	14.8	G359.1−0.9
37	1996/09/28-05:19	1996/09/28-21:55	−0.03	−2.49	29.6	GC 0−150
38	1996/09/29-13:26	1996/09/30-17:46	−0.03	−2.07	36.8	GC 0−125
39 ^c	1997/03/16-15:57	1997/03/18-07:09	−0.02	0.08	28.5	SGRA N1
40	1997/03/18-07:45	1997/03/18-17:41	0.78	1.16	9.3	SGRA N2
41	1997/03/20-21:36	1997/03/23-04:56	−0.76	−0.32	76.0	G359.1−0.2
42	1997/04/02-06:21	1997/04/02-22:53	−2.33	−0.12	14.4	GRS 1737−31
43	1997/09/15-11:57	1997/09/16-20:09	1.59	0.13	6.0	AGPS267.3−27.4
44 ^e	1997/09/19-05:28	1997/09/19-23:08	−1.00	1.00	16.7	G359.1+0.9
45	1997/09/29-07:13	1997/09/30-12:49	0.56	1.20	32.3	GRS 1739−278
46	1998/03/13-21:05	1998/03/16-09:09	1.82	0.14	8.8	AGPS267.3 S1
47	1998/09/03-04:24	1998/09/03-10:00	−1.01	−1.01	6.1	GC REG 1 N1

Table 1—Continued

Obs-ID	Date		Coordinates		Exp. ^a	Target name
	Start (UT) ^b	End (UT) ^b	l_{II} (deg.)	b_{II} (deg.)		
48	1998/09/03-10:56	1998/09/03-20:44	−0.51	−1.02	9.7	GC REG 1 N2
49	1998/09/03-20:08	1998/09/04-03:16	0.49	−1.01	9.1	GC REG 1 N3
50	1998/09/04-03:48	1998/09/04-09:44	0.99	−1.01	8.3	GC REG 1 N4
51	1998/09/04-08:40	1998/09/04-16:08	−0.51	−0.52	8.4	GC REG 1 N5
52	1998/09/04-16:04	1998/09/05-00:40	0.24	−0.52	8.4	GC REG 1 N6
53	1998/09/06-09:44	1998/09/06-18:44	0.74	−0.52	5.7	GC REG 1 N7
54	1998/09/06-18:39	1998/09/06-21:07	−0.75	0.48	3.3	GC REG 1 N8
55	1998/09/07-01:51	1998/09/07-07:35	−0.26	0.49	7.4	GC REG 1 N9
56	1998/09/07-07:51	1998/09/07-15:27	0.24	0.48	9.3	GC REG 1 N10
57	1998/09/07-15:43	1998/09/07-23:07	0.74	0.48	10.0	GC REG 1 N11
58	1998/09/07-23:03	1998/09/08-05:59	−0.51	0.98	10.0	GC REG 2 N1
59	1998/09/08-05:55	1998/09/08-11:43	−0.76	1.48	7.9	GC REG 2 N2
60	1998/09/08-11:43	1998/09/08-21:51	−0.26	1.48	9.5	GC REG 2 N3
61	1998/09/08-21:19	1998/09/09-03:43	0.24	1.48	10.0	GC REG 2 N4
62	1998/09/09-03:47	1998/09/09-18:59	0.50	0.98	14.5	UN SNR.5+1.0 N1
63	1998/09/09-18:27	1998/09/10-06:35	1.00	0.99	10.9	UN SNR.5+1.0 N2
64	1998/09/10-06:18	1998/09/10-14:06	−1.02	1.99	8.1	GC REG 2 N5
65	1998/09/10-14:54	1998/09/10-22:58	−0.53	1.99	9.7	GC REG 2 N6
66	1998/09/10-22:54	1998/09/11-05:42	−0.02	1.99	10.0	GC REG 2 N7
67	1998/09/11-04:38	1998/09/11-11:58	0.98	1.99	8.2	GC REG 2 N8
68	1998/09/11-11:26	1998/09/11-19:58	−1.42	0.00	7.2	GC REG 2 N9
69	1998/09/12-18:26	1998/09/12-23:34	0.71	1.49	7.4	UN SNR.75+1.5 1 N1
70	1998/09/12-23:18	1998/09/13-09:06	0.47	2.00	14.1	UN SNR.75+1.5 1 N2
71	1998/09/13-09:42	1998/09/15-02:50	−0.83	−0.81	60.3	THE MOUSE
72	1998/09/15-02:17	1998/09/15-09:57	−0.55	0.00	10.1	THE MOUSE off
73	1998/09/26-03:26	1998/09/26-16:26	0.57	−0.22	26.2	XTE J1748–288
74	1999/03/10-16:09	1999/03/10-22:37	−1.73	−0.50	12.4	GC REG3 N1
75	1999/03/10-22:36	1999/03/11-03:56	−1.23	−0.49	10.3	GC REG3 N2
76	1999/03/11-03:45	1999/03/11-08:13	−1.73	0.50	11.6	GC REG3 N3
77	1999/03/11-08:36	1999/03/11-14:04	−1.23	0.51	8.8	GC REG3 N4
78	1999/03/11-14:32	1999/03/11-20:00	−1.97	1.00	12.5	GC REG3 N5
79	1999/03/11-20:56	1999/03/12-01:32	−1.47	1.00	10.3	GC REG3 N6
80	1999/03/12-01:56	1999/03/12-06:48	−1.73	1.50	5.2	GC REG3 N7
81	1999/03/12-06:44	1999/03/12-12:48	−1.23	1.51	6.1	GC REG3 N8
82	1999/03/12-12:16	1999/03/12-19:32	−1.98	2.00	12.1	GC REG3 N9
83	1999/03/12-19:00	1999/03/13-00:40	−1.48	2.00	10.8	GC REG3 N10
84	1999/03/14-15:48	1999/03/14-22:32	1.28	−0.51	11.9	GC REG 4 N01
85	1999/03/14-22:35	1999/03/15-02:19	1.78	−0.51	8.5	GC REG 4 N02
86	1999/03/15-02:03	1999/03/15-09:03	1.28	0.49	6.8	GC REG 4 N03
87	1999/03/15-09:27	1999/03/15-17:55	1.78	0.49	7.3	GC REG 4 N04
88	1999/03/15-16:47	1999/03/15-22:11	0.03	0.99	9.8	GC REG 4 N05
89	1999/03/15-21:35	1999/03/16-02:19	1.53	0.99	10.8	GC REG 4 N06
90	1999/03/16-02:43	1999/03/16-09:55	2.03	0.99	5.0	GC REG 4 N07
91	1999/03/16-08:47	1999/03/16-18:11	1.28	1.49	7.5	GC REG 4 N08
92	1999/03/16-18:35	1999/03/16-23:43	1.78	1.49	10.1	GC REG 4 N09
93	1999/09/25-03:02	1999/09/25-09:26	−0.78	−1.50	9.1	GC REG 5 N7
94	1999/09/25-09:22	1999/09/25-19:10	−0.28	−1.50	9.1	GC REG 5 N8

Table 1—Continued

Obs-ID	Date		Coordinates		Exp. ^a (ksec)	Target name
	Start (UT) ^b	End (UT) ^b	l_{II} (deg.)	b_{II} (deg.)		
95	1999/09/25-19:06	1999/09/26-03:02	−2.03	−1.00	8.1	GC REG 5 N9
96	1999/09/26-02:26	1999/09/26-09:02	−1.53	−1.00	8.8	GC REG 5 N10
97	1999/09/29-13:04	1999/09/29-22:48	1.48	1.99	9.3	GC REG 4 N10
98	1999/09/29-22:56	1999/09/30-05:00	0.48	−2.01	8.1	GC REG 6 N1
99	1999/09/30-05:16	1999/09/30-12:32	0.98	−2.01	9.8	GC REG 6 N2
100	1999/09/30-12:44	1999/09/30-22:24	1.48	−2.01	9.5	GC REG 6 N3
101	1999/09/30-22:20	1999/10/01-03:24	1.98	−2.01	10.6	GC REG 6 N4
102	1999/10/01-09:24	1999/10/01-20:32	0.23	−1.51	10.2	GC REG 6 N5
103	1999/10/01-21:32	1999/10/02-01:00	0.73	−1.51	7.6	GC REG 6 N6
104	1999/10/02-01:28	1999/10/02-06:56	1.23	−1.51	6.6	GC REG 6 N7
105	1999/10/02-07:28	1999/10/02-15:16	1.73	−1.51	9.0	GC REG 6 N8
106	1999/10/02-15:36	1999/10/02-23:00	1.48	−1.01	10.4	GC REG 6 N9
107	1999/10/02-23:56	1999/10/03-05:32	1.98	−1.01	8.6	GC REG 6 N10

^aThe average exposure with GIS2 and GIS3 after the screening.

^b(Year/Month/Date-Hour:Minute).

^cGIS bit assignment of 10-8-8-0-0-5.

^dGIS bit assignment of 8-8-8-5-0-2 for high and low bit-rate data, and 8-6-6-5-0-6 for medium bit-rate data.

^eGIS bit assignment of 8-8-8-5-0-2.

Table 2. Point source list

Src-No ^a	Name ^b	l_{II}^{c}	b_{II}^{c}	(Obs-ID) ^d	F_{X}^{e}	Γ^{f}	N_{H}^{g}	ID	Category	Reference
1	AX J1734.5–2915	−1.560	1.867	(83)	3	$\gtrsim 10$	$11.0^{+3.6}_{-<11.0}$			
2	AX J1735.1–2930	−1.696	1.642	(80)	49	$1.80^{+0.73}_{-0.29}$	< 0.9			
3	AX J1736.4–2910	−1.258	1.571	(81)	10	$2.51^{+1.9}_{-0.66}$	< 1.5	HD 315992	Star	53
4	AX J1737.4–2907	−1.111	1.419	(59)	430	$1.41^{+0.52}_{-0.50}$	$1.1^{+1.1}_{-<1.1}$	GRS 1734–292	Seyfert-I	1,3,33
				(81)	310	$1.51^{+0.20}_{-0.19}$	$1.7^{+0.4}_{-0.3}$			
5	AX J1738.2–2659	0.800	2.407	(15)	1800	$2.18^{+0.03}_{-0.03}$	$1.6^{+0.1}_{-0.1}$	SLX 1735–269	Burster	7,10,12,17
6	AX J1738.4–2902	−0.917	1.280	(44)	7	$3.6^{+>6}_{-1.3}$	< 1.1	RX J1738.4–2901		53
				(59)	<13	3.6(fix)	0.0(fix)			
7	AX J1739.1–3020	−1.932	0.456	(76)	1100	$0.85^{+0.10}_{-0.10}$	$3.2^{+0.3}_{-0.3}$	XTE J1739–302		47
8	AX J1739.3–2923	−1.117	0.926	(44)	19	$1.0^{+1.6}_{-1.2}$	$1.8^{+6.0}_{-<1.8}$			
9	AX J1739.4–2656	0.979	2.199	(15)	<6	6.3(fix)	13(fix)			
				(67)	7	$6.3^{+>4}_{-5.8}$	$13^{+19}_{-<13}$			
10	AX J1739.5–2910	−0.903	1.013	(44)	4	$3.9^{+5.8}_{-1.3}$	$0.2^{+1.8}_{-<0.2}$? ^h	? ^h	18,53
11	AX J1739.5–2730	0.519	1.882	(70)	15	$1.07^{+0.98}_{-0.97}$	$0.9^{+2.1}_{-<0.9}$			
12	AX J1740.1–3102	−2.410	−0.100	(26)	<4	1.53(fix)	6.2(fix)	GRS 1737–31	BHC	9,49
				(42)	1600	$1.53^{+0.06}_{-0.06}$	$6.2^{+0.3}_{-0.2}$			
13	AX J1740.1–2847	−0.507	1.084	(58)	40	$0.55^{+0.66}_{-0.74}$	$2.6^{+3.2}_{-2.3}$	AX J1740.1–2847	Pulsar	41
14	AX J1740.2–2903	−0.725	0.931	(44)	49	$0.62^{+0.64}_{-0.40}$	$0.1^{+1.2}_{-<0.1}$	2RXP J174015.5–290333		54
				(58)	53	$-0.4^{+5.0}_{-1.1}$	< 45			
15	AX J1740.4–2856	−0.609	0.958	(58)	7	$2.66^{+1.3}_{-0.68}$	< 0.5	1RXS J174024.6–285706		50
16	AX J1740.5–3014	−1.691	0.260	(22)	25	$3.4^{+>7}_{-3.7}$	$10^{+30}_{-<10}$	SAX J1740.5–3013		53
				(76)	<18	3.4(fix)	10(fix)			
17	AX J1740.5–2937	−1.173	0.582	(77)	8	$4.6^{+>5}_{-1.4}$	< 2.3	1RXS J174034.3–293749		50
18	AX J1740.7–2818	−0.029	1.231	(29)	630	$2.10^{+0.11}_{-0.11}$	$1.9^{+0.2}_{-0.2}$	SLX 1737–282		44
				(30)	500	$2.17^{+0.16}_{-0.15}$	$2.0^{+0.2}_{-0.2}$			
				(60)	650	$2.34^{+0.21}_{-0.19}$	$2.2^{+0.3}_{-0.3}$			
				(61)	650	$2.36^{+0.31}_{-0.29}$	$2.0^{+0.5}_{-0.4}$			
				(88)	480	$2.18^{+0.19}_{-0.18}$	$1.9^{+0.3}_{-0.2}$			
19	AX J1742.5–2845	−0.201	0.668	(9)	21	$4.9^{+5}_{-1.6}$	< 1.1	1RXS J174230.4–284504		50
				(29)	<14	4.9(fix)	0.5(fix)			
				(31)	<33	4.9(fix)	0.5(fix)			
				(55)	13	$4.9^{+>5}_{-2.1}$	$0.5^{+2.0}_{-<0.5}$			
				(88)	31	$3.7^{+>6}_{-1.2}$	$0.1^{+2.6}_{-<0.1}$			
20	AX J1742.6–3022	−1.564	−0.200	(22)	31	$0.2^{+3.7}_{-1.2}$	$2.6^{+48}_{-<2.6}$			
				(68)	23	$1.9^{+>8}_{-2.1}$	$3.6^{+44}_{-<3.6}$			
				(74)	54	$0.9^{+7.6}_{-3}$	18^{+79}_{-18}			
21	AX J1742.6–2901	−0.414	0.498	(54)	<16	10(fix)	10.1(fix)	2RXP J174241.8–290215		54

Table 2—Continued

Src-No ^a	Name ^b	l_{II}^{c}	b_{II}^{c}	(Obs-ID) ^d	F_{X}^{e}	Γ^{f}	N_{H}^{g}	ID	Category	Reference
22	AX J1743.9–2846	−0.060	0.400	(55) (9) (27) (31) (39) (55) (56)	7 10 35 45 94 <8 <22	$\gtrsim 10$ $2.6^{+1.7}_{-1.0}$ >4.8 $0.23^{+0.34}_{-0.26}$ $1.87^{+1.3}_{-0.80}$ 1.87(fix) 1.87(fix)	$10.1^{+2.2}_{-5.4}$ $0.7^{+1.2}_{-0.7}$ $9.6^{+2.5}_{-2.1}$ <0.6 $0.2^{+0.5}_{-0.2}$ 0.2(fix) 0.2(fix)	2RXP J174351.3-284640		54
23	AX J1743.9–2945	−0.887	−0.113	(1) (10) (11) (20) (41)	2100 1600 1500 760 2500	$1.36^{+0.07}_{-0.07}$ $1.51^{+0.11}_{-0.11}$ $1.41^{+0.12}_{-0.12}$ $1.40^{+0.30}_{-0.28}$ $1.13^{+0.06}_{-0.06}$	$13.1^{+0.5}_{-0.5}$ $13.6^{+0.8}_{-0.8}$ $13.3^{+0.9}_{-0.8}$ $12.0^{+2.1}_{-1.8}$ $12.2^{+0.4}_{-0.4}$	1E 1740.7–2942	BHC	2,5,16,20,27,35,40
24	AX J1744.5–2844	0.041	0.307	(2) (3) (9) (12) (27) (31) (39) (55) (56)	<14 <16 <12 <15 200000 6000 50000 <40 <28	1.14(fix) 1.14(fix) 1.14(fix) 1.14(fix) $1.14^{+0.01}_{-0.01}$ $0.99^{+0.03}_{-0.03}$ $0.87^{+0.01}_{-0.01}$ 1.14(fix) 1.14(fix)	5.5(fix) 5.5(fix) 5.5(fix) 5.5(fix) $5.5^{+0.1}_{-0.1}$ $5.4^{+0.1}_{-0.1}$ $4.7^{+0.1}_{-0.1}$ 5.5(fix) 5.5(fix)	GRO J1744–28	Bursting pulsar	14,29,36
25	AX J1744.8–2921	−0.440	−0.083	(7) (8) (72)	<23 <24 910	2.12(fix) 2.12(fix) $2.12^{+0.20}_{-0.19}$	20.3(fix) 20.3(fix) $20.3^{+1.7}_{-1.6}$	KS 1741–293	Burster	43,52
26	AX J1745.0–2855	−0.049	0.113	(2) (3) (7) (9) (12) (31) (39)	<12 <40 <20 <19 18 1000 <8	2.36(fix) 2.36(fix) 2.36(fix) 2.36(fix) $2.0^{+2.1}_{-1.5}$ $2.36^{+0.16}_{-0.16}$ 2.36(fix)	11.4(fix) 11.4(fix) 11.4(fix) 11.4(fix) $13.3^{+14}_{-9.2}$ $11.4^{+0.9}_{-0.8}$ 11.4(fix)	GRS 1741.9–2853	Burster	6,32,37
27	AX J1745.6–2901	−0.079	−0.044	(2) (7) (12) (39)	200 220 780 180	$1.24^{+0.79}_{-0.44}$ $2.16^{+0.95}_{-0.71}$ $2.54^{+0.11}_{-0.11}$ $1.44^{+0.62}_{-0.53}$	$10.0^{+7.1}_{-3.3}$ $15.3^{+9.1}_{-5.6}$ $19.6^{+0.9}_{-0.9}$ $12.9^{+6.0}_{-4.3}$	AX J1745.6–2901	Burster	24,30
28	AX J1745.6–2900 ⁱ	−0.065	−0.047	(2) (7)	210 170	$2.35^{+0.34}_{-0.34}$ $2.66^{+0.85}_{-0.70}$	$7.3^{+1.3}_{-1.1}$ $8.4^{+2.8}_{-2.2}$	Sgr A	MBH ⁱ	13,15,26

Table 2—Continued

Src-No ^a	Name ^b	l_{II}^{c}	b_{II}^{c}	(Obs-ID) ^d	F_{X}^{e}	Γ^{f}	N_{H}^{g}	ID	Category	Reference
29	AX J1746.1–2931	−0.443	−0.401	(12) 3100 (39) 2700 (41) 6300 (51) 2500	320 2.35(fix) 240 $2.17^{+0.27}_{-0.25}$ 1.40 $^{+0.10}_{-0.10}$ 1.64 $^{+0.10}_{-0.09}$ 1.84 $^{+0.03}_{-0.03}$ 1.82 $^{+0.07}_{-0.06}$	7.3(fix) $7.5^{+1.1}_{-0.9}$ $5.9^{+0.4}_{-0.4}$ $6.5^{+0.4}_{-0.4}$ $6.6^{+0.1}_{-0.1}$ $5.8^{+0.2}_{-0.2}$		A 1742–294	Burster	4,28,50
30	AX J1746.3–2843	0.260	−0.031	(2) 1100 (3) 1200 (4) 1200 (5) 1500 (12) 1300 (13) 1200 (14) 1500 (21) 710 (39) 910	2.11 $^{+0.22}_{-0.21}$ 1.90 $^{+0.21}_{-0.20}$ 1.77 $^{+0.19}_{-0.19}$ 1.42 $^{+0.18}_{-0.17}$ 1.83 $^{+0.08}_{-0.08}$ 1.76 $^{+0.13}_{-0.12}$ 1.71 $^{+0.19}_{-0.19}$ 2.12 $^{+0.09}_{-0.09}$ 1.65 $^{+0.35}_{-0.33}$	$19.5^{+1.9}_{-1.7}$ $19.1^{+1.9}_{-1.8}$ $17.6^{+1.6}_{-1.5}$ $16.7^{+1.5}_{-1.4}$ $18.2^{+0.7}_{-0.7}$ $17.4^{+1.1}_{-1.0}$ $18.9^{+1.7}_{-1.6}$ $18.6^{+0.8}_{-0.8}$ $20.6^{+3.3}_{-3.0}$	1E 1743.1–2843		8,51	
31	AX J1747.0–2828	0.552	−0.025	(3) <30 (4) <12 (13) 8 (14) 8 (21) <11 (73) 15	3.0(fix) 3.0(fix) $3.0^{+2.7}_{-1.7}$ $1.9^{+4.2}_{-2.3}$ 3.0(fix) $0.0^{+1.9}_{-1.3}$	25(fix) 25(fix) 25^{+32}_{-15} $9.4^{+24}_{-9.4}$ 25(fix) $1.0^{+6.5}_{-1.0}$				29
32	AX J1747.0–2837	0.423	−0.107	(3) <39 (4) 12 (5) <39 (13) 10 (14) <9 (21) <11 (73) <17	1.5(fix) $1.3^{+>9}_{-<3}$ 1.5(fix) $1.5^{+5.0}_{-4}$ 1.5(fix) 1.5(fix) 1.5(fix)	7.8(fix) $8.8^{+38}_{-8.8}$ 7.8(fix) $7.8^{+20}_{-7.8}$ 7.8(fix) 7.8(fix) 7.8(fix)				
33	AX J1747.1–2809	0.828	0.123	(13) 4 (14) <9 (32) <14	>5.2 10(fix) 10(fix)	$1.4^{+0.4}_{-0.3}$ 1.4(fix) 1.4(fix)				
34	AX J1747.3–2809	0.867	0.070	(13) 28 (14) 15 (32) 23	$1.2^{+3.1}_{-1.8}$ $5.0^{+>5}_{-4.9}$ $9.10^{+>1}_{-7.3}$	17^{+28}_{-13} 32^{+64}_{-25} 100^{+32}_{-80}	SNR G0.9+0.1	SNR	22,34	
35	AX J1747.4–3000	−0.706	−0.894	(47) 240 (48) 1100 (71) 1700	$2.33^{+0.94}_{-0.76}$ $1.79^{+0.17}_{-0.16}$ $1.86^{+0.03}_{-0.03}$	$3.2^{+2.1}_{-1.6}$ $3.7^{+0.4}_{-0.4}$ $4.3^{+0.1}_{-0.1}$	SLX 1744–299	Burster	37,38	

Table 2—Continued

Src-No ^a	Name ^b	l_{II}^{c}	b_{II}^{c}	(Obs-ID) ^d	F_{X}^{e}	Γ^{f}	N_{H}^{g}	ID	Category	Reference
36	AX J1747.4–3003	−0.747	−0.923	(47) (48) (71)	2400 2800 3500	$2.08^{+0.14}_{-0.13}$ $1.98^{+0.10}_{-0.10}$ $2.14^{+0.02}_{-0.02}$	$5.3^{+0.4}_{-0.4}$ $5.5^{+0.3}_{-0.3}$ $5.9^{+0.1}_{-0.1}$	SLX 1744–300	Burster	38,45
37	AX J1747.8–2633	2.288	0.824	(90)	60000	$1.76^{+0.04}_{-0.04}$	$2.2^{+0.1}_{-0.1}$	GX 3+1	Burster	31
38	AX J1748.0–2829	0.663	−0.221	(4) (13) (14) (32) (53) (73)	<24 9 <21 <64 650 14	1.81(fix) 1.81(fix) 1.81(fix) 1.81(fix) $1.81^{+0.86}_{-0.79}$ $2.3^{+1.4}_{-1.1}$	7.3(fix) 7.3(fix) 7.3(fix) 7.3(fix) $7.3^{+3.8}_{-3.3}$ $5.9^{+4.3}_{-3.1}$	XTE J1748–288	BHC	23,25,39,46
39	AX J1748.3–2854	0.334	−0.492	(52)	7	$4.6^{+2.8}_{-2.8}$	$5.4^{+8.8}_{-3.9}$			
40	AX J1748.6–2957	−0.538	−1.087	(48)	16	$1.77^{+1.0}_{-0.90}$	$0.9^{+1.4}_{-0.9}$	HD 316341	Star	53
41	AX J1748.7–2709	1.878	0.328	(23) (25) (34) (43) (46) (87)	28 30 <55 <150 29 47	$3.2^{+7.7}_{-4.0}$ $2.1^{+5.1}_{-2.3}$ 3.2(fix) 3.2(fix) $3.2^{+3.6}_{-2.0}$ $1.3^{+1.3}_{-1.6}$	$8.5^{+42}_{-8.5}$ $6.0^{+22}_{-6.0}$ 10.2(fix) 10.2(fix) $10.2^{+19}_{-7.4}$ $3.7^{+5.1}_{-3.7}$	SNR G1.9+0.3	SNR	19
42	AX J1749.1–2733	1.585	0.051	(19) (23) (24) (33) (43) (46)	<13 <48 <34 15 46 59	2.1(fix) 2.1(fix) 2.1(fix) $2.1^{+4.7}_{-2.6}$ $\lesssim -3$ <9.9	25(fix) 25(fix) 25(fix) 25^{+57}_{-21} $7.4^{+119}_{-7.4}$ $3.3^{+93}_{-3.3}$			
43	AX J1749.1–2639	2.358	0.505	(25)	7300	$0.46^{+0.08}_{-0.07}$	$3.2^{+0.3}_{-0.2}$	GRO J1750–27	Pulsar	11,42
44	AX J1749.2–2725	1.699	0.108	(19) (23) (24) (33) (34) (43) (46)	290 180 160 <29 <69 <28 100	$0.76^{+0.91}_{-0.50}$ $0.10^{+1.00}_{-1.0}$ $0.9^{+5.0}_{-3}$ 0.51(fix) 0.51(fix) 0.51(fix) $0.51^{+0.73}_{-0.64}$	$15.4^{+9.6}_{-4.5}$ $4.5^{+8.1}_{-4.5}$ 19^{+50}_{-19} 10.4(fix) 10.4(fix) 10.4(fix) $10.4^{+7.0}_{-5.2}$	AX J1749.2–2725	Pulsar	48
45	AX J1750.5–2900	0.489	−0.952	(49)	9	$0.4^{+10}_{-1.2}$	< 75	SAX J1750.8–2900		21
46	AX J1751.1–2748	1.587	−0.451	(84) (85)	<9 8	2.7(fix) $2.7^{+7}_{-1.4}$	0.3(fix) $0.3^{+7.5}_{-0.3}$			
47	AX J1753.5–2745	1.912	−0.891	(107)	10	0.5^{+10}_{-3}	21^{+1000}_{-21}			
48	AX J1754.0–2929	0.467	−1.854	(98)	14	$1.2^{+4.9}_{-1.1}$	$0.4^{+9.2}_{-0.4}$			

Table 2—Continued

Src-No ^a	Name ^b	<i>l</i> _{II} ^c	<i>b</i> _{II} ^c	(Obs-ID) ^d	<i>F</i> _X ^e	Γ ^f	<i>N</i> _H ^g	ID	Category	Reference
49	AX J1754.2–2754	1.851	−1.101	(106) (107)	93 110	$3.7^{+1.4}_{-1.2}$ $2.54^{+0.34}_{-0.31}$	$4.5^{+2.8}_{-2.3}$ $2.1^{+0.6}_{-0.5}$			
50	AX J1754.5–2927	0.543	−1.938	(98)	3	$7.6^{+2}_{-3.8}$	$3.7^{+4.4}_{-2.8}$			
51	AX J1755.2–3017	−0.090	−2.482	(37)	5	$1.4^{+4.6}_{-2.4}$	$10^{+36}_{-<10}$			
52	AX J1755.7–2818	1.679	−1.586	(105)	12	$0.3^{+3.3}_{-2.4}$	< 11			
53	AX J1758.0–2818	1.937	−2.021	(101)	6	$2.1^{+8}_{-2.6}$	17^{+133}_{-17}			

^aSource No (Src-No).^bName designated.^cGalactic coordinates.^dObservation ID (Obs-ID) defined in Table 1.^eObserved X-ray flux in the 0.7–10 keV band [10^{-13} erg cm $^{-2}$ s $^{-1}$] or 3σ upper limit where the same spectral shape as that in their brightest state is assumed.^fPhoton index Γ , where $N(E)dE = E^{-\Gamma}dE$.^gHydrogen column density [10^{22} H cm $^{-2}$].^hIt may be HD 316072 or SNR G359.1+00.9.ⁱThis source is observed as spatially-extended plasma (see §5.1).

Note. — Errors are in 90% confidence.

References. — [1]Barret & Grindlay 1996 [2]Bouchet et al. 1991 [3]Churazov et al. 1992 [4]Churazov et al. 1995 [5]Churazov et al. 1996 [6]Cocchi et al. 1999a [7]Cocchi et al. 1999b [8]Cremonesi et al. 1999 [9]Cui et al. 1997 [10]David et al. 1997 [11]Dotani et al. 1995 [12]Elvis et al. 1992 [13]Falcke et al. 1999 [14]Finger et al. 1996 [15]Ghez et al. 1998 [16]Goldwurm et al. 1994 [17]Goldwurm et al. 1996 [18]Gray 1994 [19]Green & Gull 1984 [20]Heindl et al. 1994 [21]Heise 1997 [22]Helfand & Becker 1987 [23]Hjellming et al. 1998 [24]Kennea & Skinner 1996 [25]Kotani et al. 2000 [26]Koyama et al. 1996 [27]Kuznetsov et al. 1997 [28]Lewin et al. 1976 [29]Lewin et al. 1996 [30]Maeda et al. 1996 [31]Makishima et al. 1983 [32]Mandrou 1990 [33]Martí et al. 1998 [34]Mereghetti et al. 1998 [35]Mirabel et al. 1992 [36]Nishiuchi et al. 1999 [37]Pavlinsky et al. 1994 [38]Predehl & Kulkarni 1995 [39]Rupen et al. 1998 [40]Sakano et al. 1999a [41]Sakano et al. 2000b [42]Scott et al. 1997 [43]Sidoli et al. 1999 [44]Skinner et al. 1987 [45]Skinner et al. 1990 [46]Smith et al. 1998a [47]Smith et al. 1998b [48]Torii et al. 1998 [49]Ueda et al. 1997 [50]Voges et al. 1999 [51]Watson et al. 1981 [52]in't Zand et al. 1991 [53]SIMBAD [54]ROSAT(2RXP)

Table 3. Extended source list (including candidates)

Name	Src-No ^a	Size ^b	Γ ^c	kT ^d	N_{H} ^e	F_{X} ^f	X-ray Natures	Radio Natures	Refs.
Radio supernova remnants (SNRs) ^g									
G359.0-0.9		8 × 20	...	0.4 ± 0.1	1.5 ± 0.5	24	Thermal(Shell)	Shell-like	1
G359.1-0.5 ^h		~10	...	0.2 & 4	~8	10	Thermal(Center-filled)	Shell-like	1,7
G359.1+0.9 ⁱ	10	~4(?)	...	~0.7	~0	3	Soft X-rays (extended?)	Composite	
G0.9+0.1	34	< 1.5	~1.5	~2	~10	20	not resolved	Composite	
G1.9+0.3	41	< 1.5	~3	~1	~10	30	not resolved	Shell-like	
X-ray diffuse structures newly discovered.									
G359.4+0.0 ^j		~6	~2	...	12.6 ± 3.4	31	XRN	The Sgr C cloud	4
G359.95-0.05		2 × 3	...	≤1 & ~10	~6 & ~12	200	Thermal(Center-filled)	The Sgr A region	
G0.0-1.3		40 × 15	...	0.4-0.6	1.1-1.5	100	Thermal(Center-filled)	...	
G0.1-0.1 ^k		15 × 10	...	≤1 & ~10	~4 & ~6	650	Thermal & 6.4-keV line	around the Radio Arc	
G0.56-0.01 ^l	31	< 1.5	...	4-8	5-7	8	Strong iron-K	...	5,6
G0.7-0.1		~7	~2	...	83 ± 23	25	XRN	The Sgr B2 cloud	2,3
G1.0-0.1		15 × 60	~3.5	~1.0	~0.8	50	Thermal?(Center-filled)	...	

^aSrc-No. defined in Table 2, when the source is not spatially resolved with *ASCA*.

^bApparent X-ray size in unit of arcmin.

^cPhoton index when the spectrum is fitted with a power-law function.

^dTemperature [keV] when the spectrum is fitted with a thin thermal model.

^eHydrogen column density [10^{22} H cm $^{-2}$].

^fObserved flux with the 0.7-10 keV band [10^{-13} erg s $^{-1}$ cm $^{-2}$].

^gD. A. Green 1998: <http://www.mrao.cam.ac.uk/surveys/snrs/> .

^hTwo components for thermal emission are required. See Yokogawa et al. (2000) and Bamba et al. (2000) for detail.

ⁱIf the central point-like component, AX J1739.5-2910, is due to a star HD 316072 (see Table 2), the flux of the diffuse component is crucially contaminated by the emission.

^jX-ray reflection nebula (XRN), Sgr C, which is characterized with a strong neutral iron line (Murakami et al. 2001).

^kTwo components for thermal emission are required. A part of emission is overlapped with the Radio Arc.

^lThe X-ray emitting region, which was not resolved with *ASCA* (see Src-No=31 in Table 2 or Sakano et al. 1999d), was recently found to be truly extended with the *Chandra* observation (Sendai et al. 2001).

Table 4. Multi-line fit to the Sgr A diffuse plasma spectrum in 1993

Param.	Best-fit Value	Comment
Continuum		
F_x	2.0	Observed flux (10^{-11} erg s $^{-1}$ cm $^{-2}$; 2–10 keV)
L_x	2.9	Luminosity (10^{35} erg s $^{-1}$; 2–10 keV)
N_H	6.7 (5.9–7.7)	Column density (10^{22} H cm $^{-2}$)
kT	8.0 (5.4–14.7)	Temperature (keV)
Emission (K α) lines in unit of (10^{-5} photon s $^{-1}$ cm $^{-2}$)		
Si	1.5 (0.3–2.7)	(1.86 keV; He-like)
S	4.3 (2.5–6.2)	(2.45 keV; He-like)
Ar	2.5 (0.1–3.8)	(3.14 keV; He-like)
Ca	2.5 (0.3–3.6)	(3.90 keV; He-like)
Fe	<2.7	(6.4 keV; Neutral)
Fe	13 (8–17)	(6.7 keV; He-like)
Fe	3.2 (<6.7)	(6.97 keV; H-like)
$\chi^2/\text{d.o.f.}$	114.5/124	

Note. — The spectrum is accumulated from the region indicated in Figure 3 (see also text). The fit was made with the model of seven Gaussian lines and an absorbed thermal bremsstrahlung for the energy band of 1.5–10 keV. Because of the limited statistics, each line energy was fixed to the theoretical value, and the line width was fixed to zero. Uncertainties are in 90% confidence. Note that the plasma has an additional soft component below 1.5 keV.